2011

Stress Shielding Minimized In Femoral Hip Implants A Finite Element Model Optimized By Virtual Compatibility

Christian E. Feldt
University of Central Florida

STRESS SHIELDING MINIMIZED IN FEMORAL HIP IMPLANTS: A FINITE ELEMENT MODEL OPTIMIZED BY VIRTUAL COMPATIBILITY

by

CHRISTIAN E. FELDT
B.S. University of Central Florida, 2000
M.S. University of Central Florida, 2002

A dissertation submitted in partial fulfillment of the requirements
for the degree of Doctor of Philosophy
in the Department of Mechanical, Materials, and Aerospace Engineering
in the College of Engineering and Computer Science
at the University of Central Florida
Orlando, Florida

Summer Term
2011

Major Professor: Larry Chew

ABSTRACT

Bone mechanics and traditional implant materials produce a recurring problem for patients of total hip arthroplasty (THA): the bone is "shielded" from the loading it has become accustomed to over many years of development. Bone adheres to what is called "Wolff's Law", meaning it is an adaptive structure which adjusts its geometry based on the loads experienced over its life (Pearson; Goldstein). As the new femoral hip implant transmits reduced stresses to the remaining bone, bone tissue atrophies at the interface, permitting loosening of the implant, pain, and thereby obliging additional surgery to correct the issue (Meade).

In the present work, a methodology is endeavored for creating an innovative design for femoral hip implants. The approach uncouples the finite element implant model from the bone model, in order to focus solely on expected behavior within the implant while considering the varying material behavior in unique directions and locations. The implant's internal geometry is optimized in order to better match typical, intact bone conditions. The eventual design reduces extreme changes in stresses within remnant bone such that the implant will remain implanted for greater periods of time without additional surgical attention.

TABLE OF CONTENTS

LIST OF FIGURES

LIST OF TABLES

1. INTRODUCTION

Every year, over 800,000 hip replacement surgeries are completed throughout the world (Li; Kowalczyk), and every year this number increases (Pawlikowski, Skalski and Haraburda). These procedures involve replacing some or all of the bone components of the hip joint with an appropriate artificial substitute in order to correct some anatomical deficiency, whether resulting naturally or from some physical trauma. Because hip replacement surgery leaves most muscles intact on the remaining bone, many patients, with proper caution, can live a healthy, active lifestyle. These very common procedures are undoubtedly one of those most successful in orthopedics today (Hori). In spite of past achievement, limitations on hip replacement continually drive orthopedic researchers to investigate means of improvement (Chang; Evans).

The nature of health in a population is such that the more successful the medical treatment of a populace, the longer that group will live to develop additional health problems (Hori). In this case, increased longevity in a population requires that implant components must do the same. If we accept that hip implants tend to last about 15 years, we know that the many elderly recipients will not have need for implant revision surgery in their lifetime. Younger people naturally have less need for hip replacements, yet require better implant endurance if they do become patients. When a revision is essential, the previously removed bone mass leaves surgeons with less control over results; therefore, subsequent procedures are rarely as enduring as the initial (Hori; Li; Higa). The conclusion is clear: the fewer

revision surgeries necessary, the better for any patient. Many researchers are therefore investigating the factors inhibiting an implant's long-life.

Research from the last few decades has revealed a primary, limiting element: adaptation known as stress shielding. The high stiffness of typical implant materials dwarfs that of the surrounding bone (Charnley; Bundy, Bone Prosthesis and Implants; Wuh). It is said that the bone is shielded from its normal work load due to this artificial departure. Bone, being a highly adaptive material, responds over time to the new stress conditions and atrophies, by remodeling, transforming, and ridding itself of materials it senses as unnecessary (Bagge; Serbousek; Meade). The resulting problem: the implant loosens as it loses bone with which to mate. This leads to premature failures demanding revision – a more uncertain procedure now given less bone mass to work with (R. Cunningham).

The higher stiffness of implants is not the only relevant difference with bone. Bone possesses a fundamental behavioral difference in how its stiffness varies from point to point and from orientation to orientation throughout the bone structure (Bagge; Goldstein; J. L. Katz). Engineering materials such as steel, titanium, and even plastics, perform far more uniformly. Failure to consider this effect impedes development of a truly perfect implant.

In spite of the complex behavior of bone, the vast majority of implant optimizations of the past have chosen to greatly simplify the behavior of bone (Li; Simoes). To reduce calculation complexity, this biological tissue is treated like a common isotropic polymer or metal. While results to-date for some implants may be somewhat satisfactory, the changing nature of this market demands additional, distinctive analyses. Engineers must strive to

make as few concessions as possible regarding the elasticity of bone in all directions and in all positions. Considering these factors may lead to innovative implants for extended life in the human body.

This work is undertaken in order to uniquely optimize the internal geometry of femoral hip implants. To this end, we are validating a method of uncoupling 2D finite element models of bone and implant. This reduces computational demands during optimization. Consideration of variations in bone properties with location and orientation serves to produce more accurate results. The Finite Element Method is used to impose "virtual compatibility" upon the system. A variation of inverse methods, this approach balances the desire for simplified computational demands while rendering a potentially more accurate implant optimization and greater insight into future designs. Upon implantation, such an implant should experience a longer life than conventional implants, consequently reducing the need for revision surgeries.

2. FOUNDATIONS

2.1 Hip Joint Pathology

The most common hip ailment necessitating replacement surgery is osteoarthritis. This "wear and tear" arthritis affects well over three-quarters of people reaching 70 years or older (Yildiz). No physical difficulties need to manifest earlier in life, but at some stage the bone loses sufficient surface cartilage for smooth articulation inside the joint. Such arthritis may appear within shoulders, hips, knees, fingers, etc. As bone confronts bone – never a desirable encounter – significant pain develops. Surface smoothness and friction properties of bone cannot rival that of cartilage. If unresolved, wearing of the joint will progress in this manner with increasing discomfort.

While all people may at some time in their lives experience a level of joint wear due to lagging or deficient repair and replacement, at times the body itself aggravates the onset or progress of arthritis. Many conditions result from the immune system attacking the body. When this effect hastens deterioration by attacking cartilage, this is termed an autoimmune disease known as rheumatoid arthritis – a destruction of the normal joint structure producing swelling and pain.

Similar pain effects can also be produced through trauma. Imagine a dislocation or fracture of the hip. Recovery can occur in the short term, but this would not obviate long term difficulties. Even upon healing of the joint, small irregularities in hip function mechanics become amplified over time and they can create greater future wear of the joint.

Years of pain free living would give way to ever increasing discomfort as the latest joint arrangement degenerates. For this reason, trauma sufferers should always be wary of future complications from their injuries and follow sound medical advice to maximize successful healing.

Traumatic injuries can endanger joints in ways beyond simply hip function mechanics. Loss of nutrients can also promote arthritis. The bone mass may perfectly heal following an accident while essential internal structures may not. If blood vessels are damaged within the bone, essential blood nutrients could be deficient. If true for active regions of the bone, localized death or avascular necrosis can result. Under such conditions, tissue is unable to effectively grow or heal in response to daily activities; problems with cartilage can be an obvious consequence. As the situation progresses, a person experiences acute pain without apparent cause. Little irregularity would be noted on X-Rays since avascular necrosis masks itself stealthily from such diagnoses. In fact, it is often by process of elimination that this condition is diagnosed.

Clearly, sufferers of traumatic joint injuries have much to be cautious of, but whatever the cause of the original malaise, these degenerations of the hip often promote awkward gait patterns. While alleviating some pain, these gaits may in fact adversely affect the joint. In other words, by trying to avoid discomfort, a person may move in an unusual fashion which damages the joint. Furthermore, the rubbing of bone, as an aberrant articulation, tends to produce bony spurs at the fringes of bone movement. As these barbs accumulate, many patients experience greater limitations of movement along with more

intense pain. Even with a successful surgical procedure to remove the bone spurs, the underlying cause would only produce more over time.

Since cartilage cannot be replaced on the bone surface, one solution to the preceding problems would be surgical removal of some or all of the components of the hip joint to be replaced by an implant. The following sections will provide a foundation for understanding the mechanics of this important joint to recognize suitable bone/implant interface behaviors.

2.2 Anatomy / Physiology

To begin developing a proper analysis for hip replacement, it is important to fully understand its construction. The following sections will discuss composition, cellular configurations, arrangement of joint structures, and modes of operation in order to better grasp the physiology of this joint at all dimensional levels.

2.2.1 Molecular Structure

Bone possesses an interesting mix of inorganic and organic parts, yet is largely dominated by an apatite mineral (one of the few minerals used and produced by biological systems). While 10% of the bone mass is water, about 30% of the bone mass is organic, with the remainder being an impure form of calcium phosphate called hydroxyapatite (Pearson; Jee). The impurity results from the presence of chloride, fluoride, carbonate, sodium, strontium, magnesium, and potassium scattered throughout the structure (Gray).

The highly crystalline ceramic is described by the chemical formula, $3Ca_3(PO_4)_2X\ Ca(OH)_2$, which is sometimes identically written as $Ca_{10}(PO_4)_6X\ (OH)_2$ where "X" denotes the aforementioned impurities (Fung). Aside from its presence in bone, this mineral appears naturally in teeth and whale baleen, while related calcium phosphates can even appear in natural rock as well (Rhoades; Jee).

The organic component of bone is composed of large quantities of amino acids. The dominant amino acids within bone proteins are proline, glycine, hydroxylysine, and hydroxyproline, a proline derivative. The distinctive shape and composition of these groups readily permits integration to form the most abundant protein in the human body, a complex molecule called collagen (L. d. Silva; Fung).

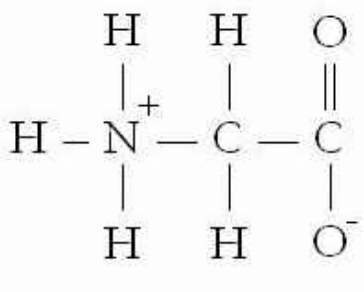

Figure 1. Molecular structure of glycine, the most common amino acid within collagen

The collagen molecule possesses 3 strands of amino acids twisting about one another in a right-handed fashion to form a triple helix, while each individual strand twists itself in the left-handed direction. Note that standard screws twist in right-handed fashion. For this arrangement, every third molecule on the chain must be an inward facing glycine. Only

glycine fits in these positions to create the tight bonds responsible for the molecular strength particular to collagen. A strand's remaining positions could be occupied by proline, hydroxyproline or to a lesser degree, hydroxylysine. Any other amino acids are present much less frequently (Fung).

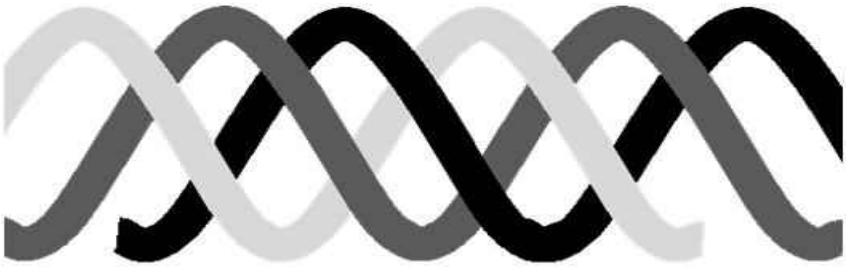

Figure 2. Tropocollogen molecule with its 3 peptide chains twisting in right handed fashion

While the glycine regularity is a necessity, the placement of the remaining amino acids varies to create numerous varieties of collagen. Throughout the body, collagen types differ in this arrangement of amino acids, providing appropriately specific mechanical characteristics to body tissues, whether it is muscle, tendon, ligament, skin, or bone. While over a dozen types of collagen exist (appropriately dubbed I, II, III, etc.), bone makes primary use of type-I along with trivial quantities of several others (Fung).

A fundamental tropocollagen molecule would measure approximately 15 atoms in diameter and 300nm in length, containing thousands of amino acid molecules. These tropocollagen threads gain complexity by clustering large numbers in parallel. Additional cross linking bonds hold the structure together and create much larger banded collagen fibrils with typical diameters between 50nm and 120nm. These bands indicate regular axial

periods of beginning/ending tropocollagen molecules and repeat approximately every 65nm (Fung).

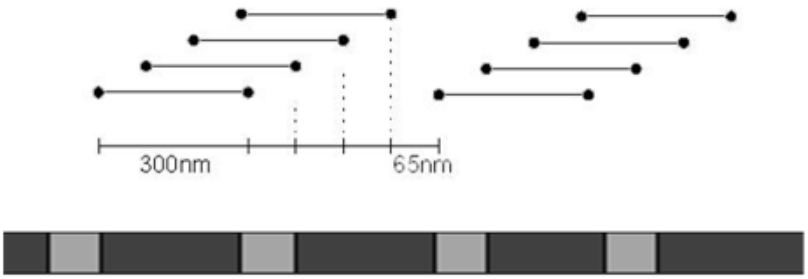

Figure 3. Arrangement of tropocollagen molecules merging to produce 65nm bandwidths in a collagen strand

Within the spaces between molecules of the fibril exist what are sometimes gaps called “hole zones”. These gaps house the aforementioned hydroxyapatite ceramic crystals. The minerals filling the zone greatly increase the stiffness of the resulting fibril. This complex composite architecture, fundamental tropocollagen molecules in league with inorganic bone mineral, is known as a mineralized collagen fibril. This synergy of inorganic and organic materials is the building block of what is called the bone matrix; this combination of materials with different properties produces a composite material with an excellent combination of properties (Pearson; Fung; Rhoades; L. d. Silva; Cowin, The Mechanical Properties of Cortical Bone Tissue).

This matrix can be arranged in two major ways. Mineralized fibrils can be woven in arbitrary directions or tend toward parallel layers. An arbitrary arrangement generates more uniform mechanical properties and is seen most often in childhood growth or in fracture

healing when growth is more rapid. As adulthood approaches, the presence of random arrangements wanes in favor of parallel architecture – a lamellar configuration which lends itself to greater divergence in properties from one direction to the next. This is why age and usage are such key contributors to the remodeling of bone matrix. The cause of this adaptation is found mixed within these layers of bone tissue: the bone cells (Fung).

2.2.2 Cellular Structures

While, at any given moment, the presence of various bone cells in bone does not noticeably influence bone properties, their steady and perpetual biological transactions certainly are of great importance. Each cell continually operates to maintain bone life by detecting bone status, removing old bone, and exploiting the properties of organic and inorganic molecules to build new bone. Three cell types accomplish these tasks: osteoclasts, osteoblasts, and osteocytes (Rhoades; Bouvier; Majeska; Jee).

Osteoclasts are a key component in bone health allowing for a healthy exchange of new and old bone mass. Large cells with multiple nuclei, osteoclasts are sometimes referred to as “bone eaters” and rest on or within cavities produced by dissolution of bone near mineral surfaces. These cavities are known as Lacunae of Howship. When need arises through trauma, disease, or wear, osteoclasts are capable of extending a foot-like member, called a podosome, in order to slide toward its next meal. Tunneling in all directions, continually producing new lacunae, osteoclasts always find additional old bone available for ingestion. Of special note is the ruffled boundary of the osteoclasts (Bouvier). The

enhanced surface area of the cell promotes superior interfacing with retiring bone. Outside the ruffled boundary, at the bone/cell surface contact, a seal forms around the volume (Pearson; Rhoades). This optimizes the rate of chemical reactions for its necessary task – which requires dissolution of inorganic and organic material (Majeska).

Firstly, several ions (primarily hydrogen) are released to establish an acidic domain for splintering the original hydroxyapatite mineral into calcium ions and phosphate groups which are readily absorbable for future expulsion. Subsequently, hydrolytic enzyme diffusion (released by cell lysosomes) facilitates dissolution of the organic collagen and bone cells (Pearson). This consumption process is tightly regulated by the body, and it is worth noting that an enzyme irregularity within osteoclasts is responsible for the bone condition known as osteoporosis (diminished bone density resulting from a bone interchange imbalance). Certainly, the consequences of osteoclasts working alone would be disastrous, and the body requires a proper balance with a cellular counterpart: the osteoblast (Majeska).

While an osteo**c**last **c**onsumes, its counterpart, the osteo**b**last, **b**uilds. Much smaller than osteoclasts, these cells cluster in tight cellular sheets blanketing the exposed bone gaps within tunneled lacunae following the feasting by its functionary foil. Always appearing in proximity to one another, the osteoblast communicates with its big brother to better guarantee effective exchange rates. When chemical signals indicate that an osteoclast has completed consumption, groups of osteoblasts mobilize to begin formation of new tissue. Their ribosomes (protein assembly features) produce tropocollagen and release it at the site of new bone. Several other external processes (forms of polymerization and proteolysis)

then encourage the more complex fibrils to materialize from the tropocollagen pieces (Majeska; Gray).

Prior to the minerals being introduced, these liberated molecules are known as osteoid. In order to complete the bone matrix, the osteoid under construction now requires the help of specialized osteoblast compartments (called vesicles) to produce the bone mineral. These compartments produce unstructured calcium phosphate from within. When sufficient in quantity, the vesicle ruptures and spews its contents into the extracellular space. Soon after, the osteoblasts release activators in the space in order to initiate crystallization of the mineral into the more complex hydroxapatite form, which completes fabrication of the matrix (Bouvier; Pearson; Majeska).

In the course of producing bone, an osteoblast frequently encapsulates itself within the matrix it creates. When this occurs, the osteoblast transforms in function and moniker: it is now an osteocyte, but it still possesses an important occupation. These star shaped cells are the most abundant bone cell and communicate with one another via tiny conduits called canaliculi, which also facilitate nutrient and waste exchange (Bouvier). Isolated as they are, osteocytes can do little to individually maintain bone tissue, yet these cells are able to detect possible faults for remodeling. With chemical signals, the osteoblasts and osteoclasts can then be directed to damaged sites to begin this process (Majeska). It is as if the old, wise osteocytes, no longer young and mobile, now are prostrate, yet attentively supervising the work of the younger bone cells .

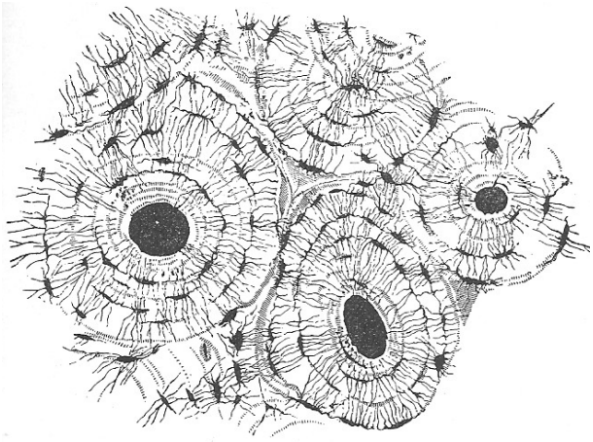

Figure 4. Transverse slice of dense, cortical bone showing the canaliculi and small star-shaped osteocytes

After osteoclasts have eaten old bone, and as the osteoblasts spew forth minerals and crystallize them around the collagen molecules, a very specific arrangement results. The architectural system of structures resulting from this activity is known as the Haversian system. The primary unit of these systems, named an osteon, is about 200-microns in diameter and 2mm in length. This system is much like the rings of a tree, having many long, cylindrical, concentric layers of bone tissue with a 50-micron diameter canal at its center. This canal encloses essential structures like blood vessels, nerves, bone cells, and the aforementioned canaliculi, for movement of nutrients and waste products (Fung; Majeska).

Incredibly, with the osteoblasts, osteoclasts, and osteocytes in constant operation, the remodeling process manages to replace 20% of our skeletons annually. Such fast operations are of great importance when it comes to injuries, but even more so when considering the tendency to produce inevitably oriented structures. We can certainly understand why

significant changes to bone usage (as by presence of an implant or low gravity environment in space) may confound this cell synchronization that typically works so well for our benefit. Examination of bone at a larger scale will further foster understanding of this concern (Fung).

2.2.3 Bone Matrix Structure

Our skeletons are composed of two subcategories of bone: cancellous bone and cortical bone. While the spongy cancellous bone fills the interior – predominantly with long bones like the humerus (upper arm) or femur (upper leg), the dense cortical bone occupies exterior surfaces (Gray). Much like the structural I-beams in a building, this arrangement maintains acceptable mechanical resistance to bending while reducing total mass of the bone (Fung). In this configuration, our bodies are strong enough to run, ski, or perform gymnastics while leaving us light enough for our muscles to reasonably control.

The Haversian system previously discussed pertains in particular to cortical bone. The osteons of this system have been woven into compact layers, or lamellae, with very low porosity (the ratio of the volume of the pores or interstices of a substance to the total volume of the mass). Often, cortical bone is defined as having less than 30% porosity. The resulting approximate density of $1.85 g/cm^3$ (near the density of aluminum or magnesium) means that this dense form holds well over 75% of human skeletal mass (Jee; Fung).

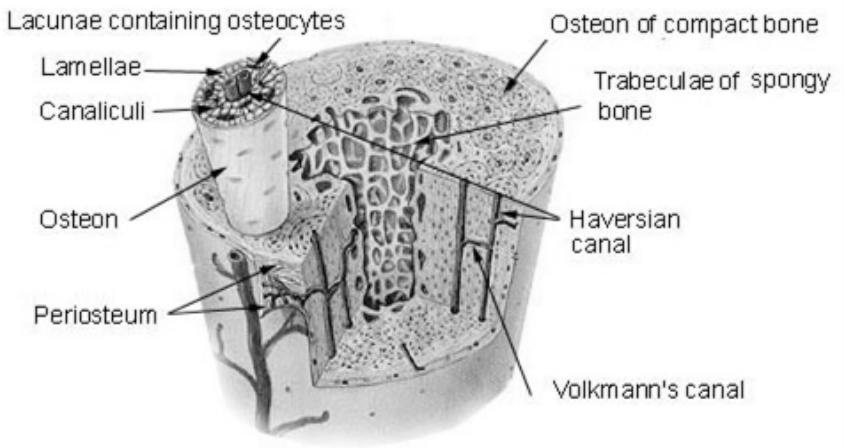

Figure 5. Dense and cortical bone tissue with features

Cancellous bone, or trabecular bone, on the other hand, is organized as a highly porous solid, similar to some types of wood or cork (Gray). The disorganized network of rods and plates produce large spaces such that porosity is greater than 70%. The density of this sparse bone ranges from 0.1 g/cm^3 to 0.6 g/cm^3, depending on the region. Notice that there is an undefined bone porosity range between 30 and 70 percent. Little skeletal bone possesses such intermediate porosity, and most of this is a minuscule transition region between cortical and cancellous bone. This makes distinction between bone types less problematic (Jee).

Within some bones, like the femur, humerus, and sternum, red bone marrow fills the spongy bone cavities. This marrow contains stem cells which are essential for the production of blood and immune system components. Other bone cavities contain yellow

marrow, which is composed of fat tissue. Neither marrow type is structurally significant, and, therefore its properties are often neglected from mechanical analyses (Jee).

2.2.4 Joint Structure

The human hip joint is classified as a ball and socket joint with the head of the femur (ball) articulating within the acetabulum (socket) of the pelvic girdle. Tightly embraced in this socket by extensive body tissue, the femur smoothly rotates, permitting a great range of motion with great strength. There are extensive bone and soft tissue features to optimize this important motion; each will be briefly discussed (Gray; Moore).

Figure 6. An encapsulated hip joint (Gray)

The acetabulum is a confluence of several bones, the ischium, the ilium, and the pubis, which are often considered one complete bone due to their rigid unions. These three

parts meld at the center of the pseudo-spherical acetabular cavity. At the inferior (lower) socket position lays a gap in the enclosure known as the acetabular notch (Gray; Moore).

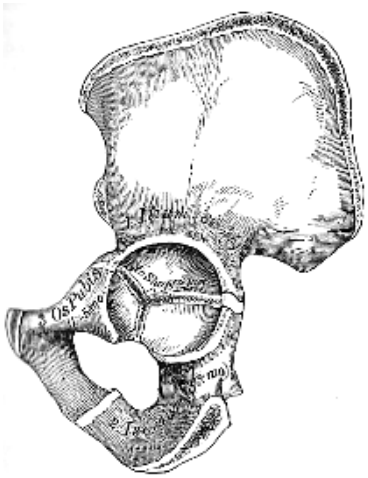

Figure 7. A pelvis shown from the lateral view, in which the convergence of three bones in the hip socket is visible (Gray)

To cushion the femoral head, the acetabular fossa (the hip socket) possesses a fat-pad covered in a membrane. All of the area surrounding this pad is covered by articular cartilage to improve surface sliding during motion. The fat-pad on the fossa predominantly serves as a dynamic impact and articulation buffer. Between the fat-pad and the acetabular notch, lies the ligament of the head of the femur (LHF). This ligament connects the acetabulum to a central point on the femoral head. While little strength or stability arises from its presence during typical motion, this ligament serves an important function by channeling blood vessels to nourish bone features. While the LHF does resist hip dislocation to some degree, hip stability is generally better served by other components (Gray; Moore).

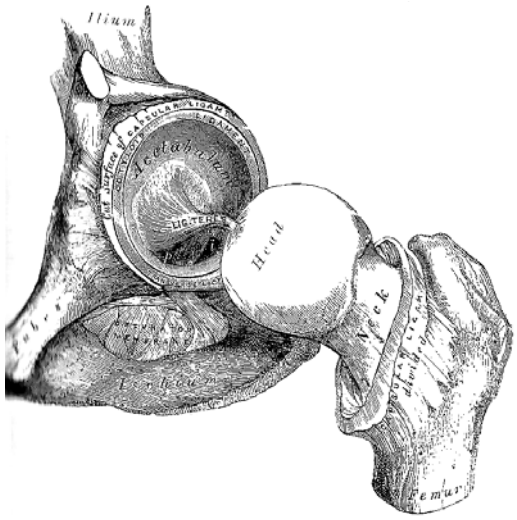

Figure 8. The left hip joint exposed, showing the LHF connecting the femur

The interior features of the acetabulum establish a smooth, softened environment for femoral rotation, yet lack stability. The joint requires more enclosure because the bone rim of the acetabulum does not fully envelop the femoral head. The acetabular labrum serves this purpose by extending a cartilaginous rim around the socket to better apply inward pressure to the femoral head. As a result, over half of the head is encapsulated, and dislocation would require a major breach of this tissue (Gray; Moore).

Additional ligaments surround the fully seated joint to further maximize stability. The iliofemoral, ischiofemoral, and pubofemoral ligaments completely surround the head and neck of the femur connecting the base of the femoral neck to the outer edge of the acetabular rim. The name of each ligament indicates which portion of the pelvis connects to the femur ("iliofemoral" connects the ilium to the femur). Within this 360° fibrous capsule of ligaments, lies a capsule of lubricating fluid known as a synovial membrane. This

capsule even extends within the socket sufficiently to surround the LHF to protect it from possible impingement. Synovial capsules of this type are copious in all joints of the body (Moore), and by some measurements produce low enough friction to rival wet ice on wet ice (Fung).

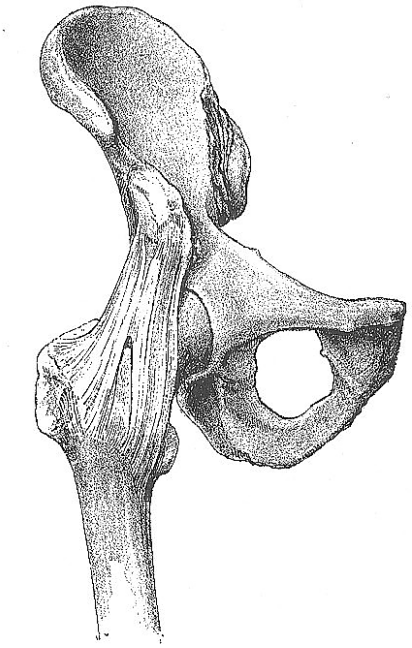

Figure 9. Right hip joint secured by the ilio-femoral ligament which joins the femur and ilium (Gray)

Farther from the hip joint, the femur possesses numerous additional features important to human mobility. Near the base of the neck of the femur originate two bony growths: the greater and lesser trochanters. These bulges provide additional areas for muscle attachment, and given the number of muscles required for leg motion, this is no trivial rationale. Mechanical analyses reveal another benefit of these two critical features:

their increased distance from the central shaft reduces the required force for rotation of the joint. This is evident in lever mechanisms where position of the load, fulcrum, and applied forces determine forces necessary to create motion. Throughout the body, muscles often attach to prominences, ridges, or tubercles to attain just this effect – to ease the workload of the acting muscles in generating rotation (Gray; Moore).

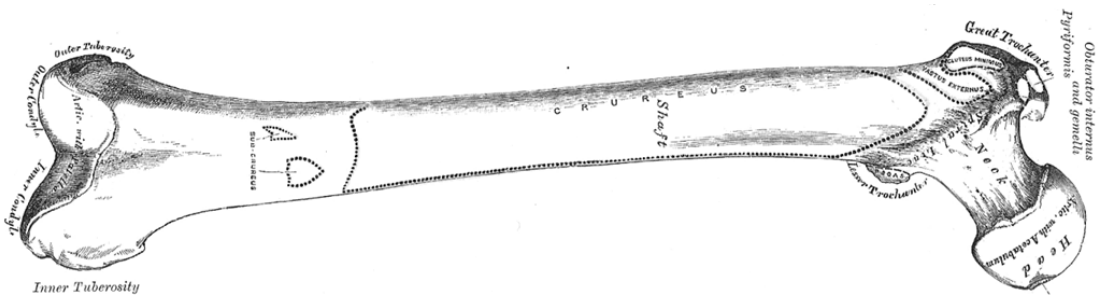

Figure 10. Anterior, right femur with important proximal features - the head, neck, greater and lesser trochanters (Gray)

The femur is the largest and strongest bone within the body. Its length is about 1/4th of the total body height. The neck of the femur forms approximately a 130° angle with the shaft (but this value varies greatly with the individual). Its cylindrical shaft (known as the diaphysis) provides great strength in axial loading and bending due to its composite construction: the aforementioned cortical and cancellous bone types are distributed within the femur in optimum proportions for demands of use (Anatomy and Biomechanics of the Hip Relevant to Arthroplasty; Gray).

Within the diaphysis, cortical wall thickness is approximately 25-40% of shaft diameter, and this surrounds a medullary cavity full of yellow marrow. More proximally, the cortical thickness reduces gradually until a uniform 1-2mm shell encases the head, neck,

and trochanters of the upper extremity. Within that same upper extremity, cancellous bone occupies the remaining space, and because the cortical layer is so thin, cancellous bone is an essential structural part of the proximal femur (Anatomy and Biomechanics of the Hip Relevant to Arthroplasty; Gray).

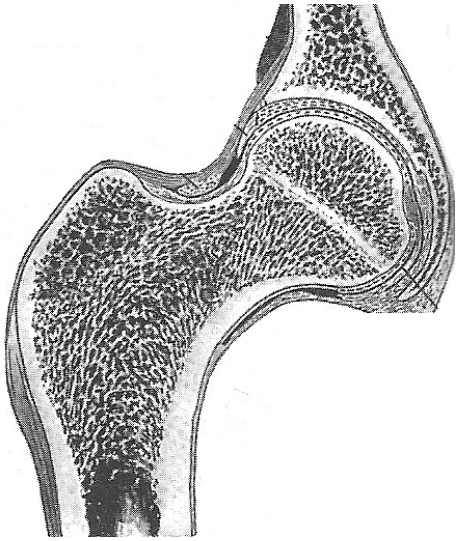

Figure 11. A slice of a human hip joint indicating the varying cortical shell, proximal cancellous bone structure, and medullary cavity

In using medical terminology, muscles have an "insertion" and "origin". The fibers originate on the less mobile bone feature while it inserts on the more mobile bone feature. For example, the quadratus femoris originates on the ischial tuberosity of the pelvis and inserts on the greater trochanter of the femur because the pelvis is relatively stationary compared to rotation of the femur. Over 30 other muscles originate or insert somewhere on the femur, but since our primary focus is the proximal femur (closer to the body center), it is more prudent to consider those muscles that insert or originate there. With these muscles

(and more) working properly, the hip joint possesses phenomenal strength and mobility (Moore)

Table 1. A small number of the muscles relevant to the proximal femur along with their functions in the body

MUSCLE	ACTION
Psoas Major	Flex vertebral column laterally; flex trunk
Iliacus	Flex and stabilize hip with psoas major
Gluteus Maximus	Hip extension; externally rotate the hip
Vastus Lateralis	Knee extension
Vastus Medialis	Knee extension
Vastus Intermedius	Knee extension
Pectineus	Externally rotate the hip; adduction
Obturator Externus	Externally rotate the hip; adduction
Piriformis	Abduction
Quadratus Femorus	Externally rotate the hip; adduction

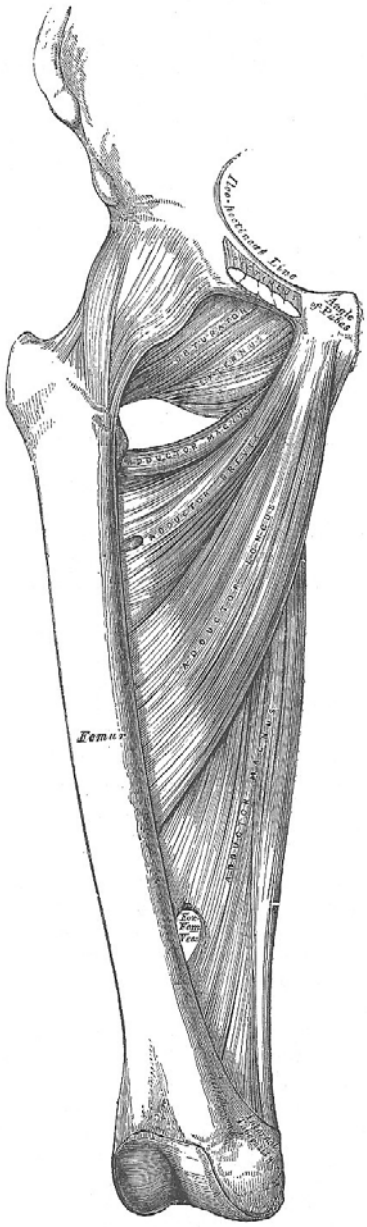

Figure 12. Anterior view of the right femur showing many of the deep muscles responsible for femoral adduction (Gray)

2.3 Kinesiology & Dynamics

Kinesiology is a science of the relationship between movement of the human body and the related physiological processes. Extensive biomechanical analysis of human movement has been carried out over the years with the goal being a better understanding of the internal workings of the relevant joints. For some, this means improved athletic performance through optimization of muscle usage and joint loads. Other researchers seek knowledge to better design therapeutic assist devices, artificial implants, or prostheses. The vast majority of research involves walking, stair climbing, or rising from seated positions. In the current work, some of the more significant hip joint movements will be examined since this affects the feasibility of designing an implant to behave in a natural way.

In a study by Heller (Musculo-skeletal loading conditions at the hip during walking and stair climbing), several patients were thoroughly analyzed while walking and climbing stairs. Each patient had undergone total hip replacement. The dominant force at the hip during walking was axial compression. This valued as high as 300% of bodyweight at 10% of stride after heel strike. This means that the opposing foot has left the ground, none of the body weight is shared, and bodyweight is multiplied due to dynamic effects. Remaining forces were 100% of bodyweight or less. Each of the patients in this study exhibited close agreement to these measures.

Kowalczyk (Design Optimization of Cementless Femoral Hip Prostheses Using Finite Element Analysis) attempted to optimize a design based on micromotion of the implant. All materials were isotropic and several loading scenarios were used in order to

evaluate a few properties of the implant: length, porous region, and winglet dimensions. Results indicated a medium length implant with a significant porous region for ingrowth produces the best outcome.

In 2001, Anderson (Dynamic Optmization of Human Walking) examined human walking gait with a three-dimensional model of the body. This work discovered a maximum ground reaction loading during walking between 750N and 1000N while the perpendicular loads are much smaller. Consider, however, that these are total loads rather than the load experienced by any particular body tissue, which could be more or less in the femur.

Heller obtained estimates of moments and forces on the hip joint during stair climbing. For the 4 test patients, internal/external rotation moment was almost completely negligible. For these same patients, maximum flexion/extension moment tended to be during extension of the hip and valued between 7.5 and 15 percent of body weight times meters (therefore a 500N person could have a maximum extension moment of 50Nm). Maximum ab/adduction tended to occur very close to maximum extension moment. The maximum values ranged about 5 to 8 % of body weight times meters, always in abduction.

In virtually all the studies investigated, at least two bodyweights were applied to the head of the femur at a steep angle. The angle tended to make the axial loading component three times more than the perpendicular components of force.

2.4 Stress

Quantities like energy or temperature are considered zero-order tensors. This means that they are numerical values devoid of any directional significance. Vectors, like velocity or force or acceleration, are called first-order tensors. Such tensors require three values to properly indicate orientation in space rather than just a magnitude. There also exist second order tensors, which we will discuss as they pertain to stress and strain (Cowin, Mechanics of Materials; Boresi and Chong).

Figure 13. Opposing, balanced forces creating axial stress in the x-direction

$$\sigma_{xx} = \frac{F_x}{A_\perp} \tag{2.1}$$

Stress is a force per unit area. The simplest system would involve stress caused by a single force on a rod. If so, the stress is found by dividing the force by the perpendicular cross section of the rod. It is this area which must bear the burden of the applied load. If another pair of balanced forces were applied in another direction, a completely unique stress would develop within the structure (Cowin, Mechanics of Materials; Beer; Fung; Boresi and Chong).

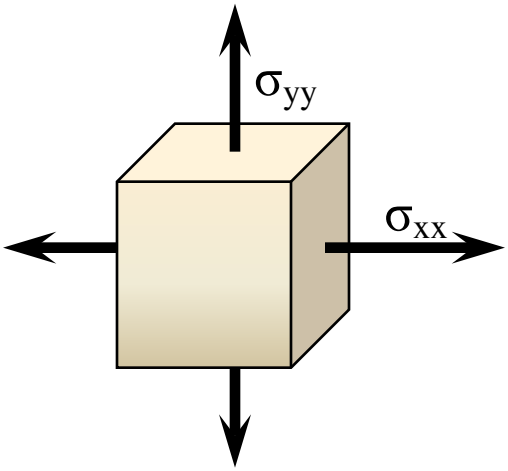

Figure 14. Biaxial stress state

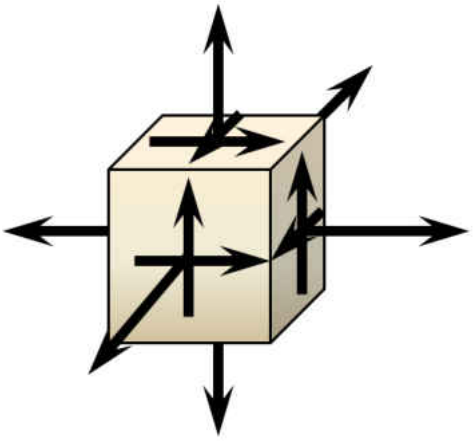

Figure 15. Fully stressed point possessing six unique values

A fully loaded cube (or a point represented in this manner) would include six faces and would show 18 stress values on the various surfaces; however, equilibrium demands that each stress possesses an identical partner on the opposing side of the cube. Furthermore, rotational equilibrium demands that many shear stresses must be balanced to prevent rotation. Therefore, a fully loaded stress state requires, at most, six unique values for a complete portrayal. Note that a stress is named by two indices: the first indicating

which face being acted on with the 2nd indicating the direction of the stress (Cowin, Mechanics of Materials; Beer; Fung; Boresi and Chong).

$$\sigma = \begin{bmatrix} \sigma_{xx} & \sigma_{xy} & \sigma_{xz} \\ \sigma_{yx} & \sigma_{yy} & \sigma_{yz} \\ \sigma_{zx} & \sigma_{zy} & \sigma_{zz} \end{bmatrix} \quad \sigma_{xy} = \sigma_{yx}, \quad \sigma_{xz} = \sigma_{zx}, \quad \sigma_{yz} = \sigma_{zy} \qquad 2.2$$

Stress, when expressed as a 3 by 3 matrix of values, follows the rules of a 2nd order tensor. This indicates that it obeys specific rules regarding its manipulation, just as vectors must obey specific rules (Fung). If a uniformly stressed structure is cut at an angle, the loading on the new face is actually a vector of stress values known as traction. Obtained from equilibrium, traction indicates how much of the loading per unit area is experienced in each of the coordinate directions. Traction is sometimes referred to as a "stress vector" (Cowin, Mechanics of Materials; Beer; Reddy; Boresi and Chong).

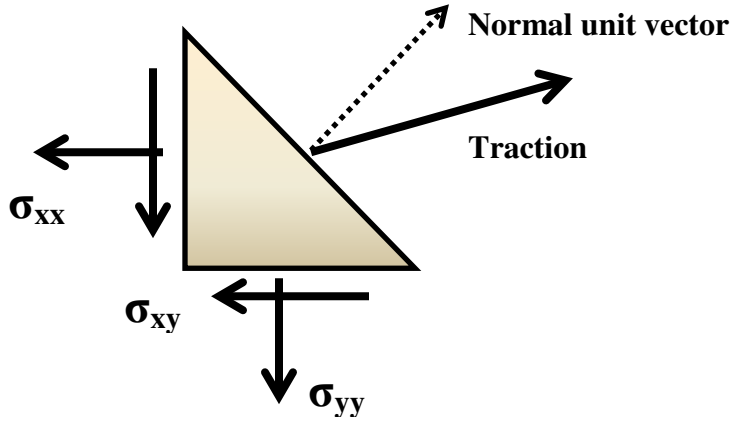

Figure 16. Traction exists on any arbitrary orientation within a stressed point

$$\left[\sigma\right]\cdot\left\{\hat{n}\right\}=\left\{T\right\} \tag{2.3}$$

$$\left\{T\right\}\cdot\left\{\hat{n}\right\}=\sigma_{normal} \tag{2.4}$$

Finding traction is readily achievable. With the stress state known for the standard coordinate system, multiplying by the unit normal vector produces traction on the face of interest. Keep in mind that in three dimensions, the six stress values produce only three traction components. In planar problems of two dimensions, three stress values produce only two non-zero traction components (Cowin, Mechanics of Materials; Beer; Boresi and Chong). This means that information is lost when converting from stress to traction. If traction is known, it is not possible to extract the full stress state without additional information.

2.5 Strain

Any applied stress will produce a distortion to a system. Strain is a unitless value representing these deformations of a solid. These distortions can be in size and/or shape. Similarly to stress, general strain occurs in three dimensions, and any point in space can experience six unique values for strain (Cowin, Mechanics of Materials; Beer; Fung; Boresi and Chong).

$$u=x_2-x_1 \quad v=y_2-y_1 \quad w=z_2-z_1 \tag{2.5}$$

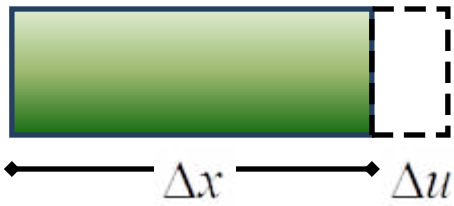

Figure 17. Uniform normal distortion producing a size change in a structure

It is first necessary to define displacement values using initial and subsequent positions as shown in equations 2.4. From these displacements, partial derivatives yield the six independent strain values. Notice that normal strains represent distortions along a single direction while shear strains represent angular distortion (Cowin, Mechanics of Materials; Beer; Fung; Boresi and Chong).

$$\varepsilon_{xx} = \frac{\partial u}{\partial x} \quad \varepsilon_{yy} = \frac{\partial v}{\partial y} \quad \varepsilon_{zz} = \frac{\partial w}{\partial z} \tag{2.6}$$

$$\varepsilon_{xy} = \left(\frac{1}{2}\right)\cdot\left(\frac{\partial u}{\partial y} + \frac{\partial v}{\partial x}\right) \quad \varepsilon_{xz} = \left(\frac{1}{2}\right)\cdot\left(\frac{\partial u}{\partial z} + \frac{\partial w}{\partial x}\right) \quad \varepsilon_{zy} = \left(\frac{1}{2}\right)\cdot\left(\frac{\partial w}{\partial y} + \frac{\partial v}{\partial z}\right) \tag{2.7}$$

With any simple, uniform distortion, we can easily gauge a finite displacement and divide this value by an original dimension to calculate strain. This displacement may be along a given dimension or perpendicular to it. All points within such figures would experience the same strain. If the strains are not uniform, these Δ values become infinitesimally small and are represented best by partial derivatives as stated previously (Cowin, Mechanics of Materials; Beer; Boresi and Chong).

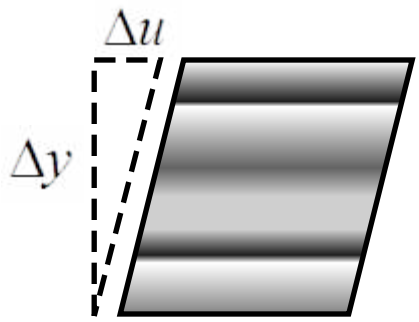

Figure 18. Shear distortion producing a shape change of a structure

Strain, like stress, can be written as a 3 x 3 matrix, but because only six values are unique due to symmetry, it is sometimes convenient to write these as an array of distinctive values. This is why the strain definitions show only three normal and three shear expressions. Any term with subscript "xy" possesses equivalence with a term of subscript "yx" (Cowin, Mechanics of Materials; Beer; Boresi and Chong).

$$\varepsilon = \begin{bmatrix} \varepsilon_{xx} & \varepsilon_{xy} & \varepsilon_{xz} \\ \varepsilon_{yx} & \varepsilon_{yy} & \varepsilon_{yz} \\ \varepsilon_{zx} & \varepsilon_{zy} & \varepsilon_{zz} \end{bmatrix} \rightarrow \varepsilon = \begin{Bmatrix} \varepsilon_{xx} \\ \varepsilon_{yy} \\ \varepsilon_{zz} \\ \varepsilon_{xy} \\ \varepsilon_{yz} \\ \varepsilon_{zx} \end{Bmatrix} \qquad 2.8$$

2.6 Stress-Strain Relationships

For one-dimensional stress problems, a stress in some direction produces a strain in the same direction – but also in perpendicular directions. If we first graph this relationship for the major axis, we can search for a linear region in order to relate stress with strain. This

slope is called modulus of elasticity. Additionally, we can examine effects in the perpendicular directions (Cowin, Mechanics of Materials; Beer).

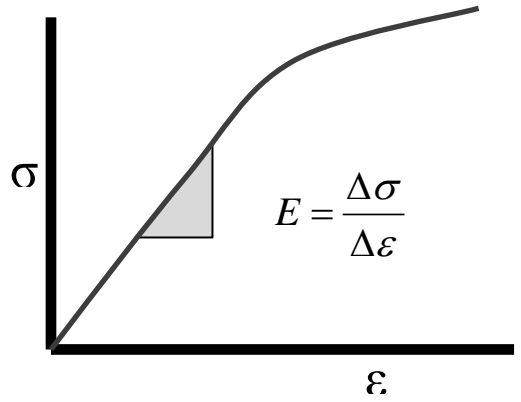

Figure 19. For 1D loading, the stress/strain curve with a common linear region of slope E

Anytime a strain is produced in one direction, strain develops in a perpendicular direction. For most materials, expansion in one direction produces contraction in others. The negative ratio of these strains is called Poisson's ratio (ν). The modulus of elasticity and Poisson's ratio are the two minimal, necessary parameters for determining the complete behavior of any material (Cowin, Mechanics of Materials; Beer).

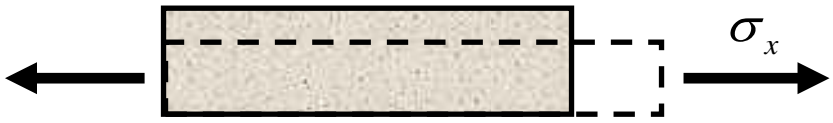

Figure 20. Uniaxial stress produces strain in multiple directions

$$\sigma_x \quad \rightarrow \quad \varepsilon_x \quad \rightarrow \quad \varepsilon_y \qquad\qquad \upsilon = -\frac{\varepsilon_y}{\varepsilon_x} \tag{2.9}$$

Some materials excel at resisting shear distortion while others possess great stiffness in linear distortion. Many materials – biological tissue in particular – behave vastly differently depending on which direction we examine. If extensive experiments are conducted in all directions for both normal and shear distortion, it is possible to obtain multiple moduli of elasticity and multiple Poisson's ratios. From this information, it is possible to create a linear matrix relationship between stress and strain. The linear relationship between the stress and strain arrays demands 36 empirical coefficients (Cowin, Mechanics of Materials; Boresi and Chong; J. L. Katz).

$$\{\sigma\} = [C] \cdot \{\varepsilon\} \quad \rightarrow \quad \begin{pmatrix} \sigma_{11} \\ \sigma_{22} \\ \sigma_{33} \\ \sigma_{12} \\ \sigma_{13} \\ \sigma_{23} \end{pmatrix} = \begin{bmatrix} c_{11} & c_{12} & c_{13} & c_{14} & c_{15} & c_{16} \\ c_{21} & c_{22} & c_{23} & c_{24} & c_{25} & c_{26} \\ c_{31} & c_{32} & c_{33} & c_{34} & c_{35} & c_{36} \\ c_{41} & c_{42} & c_{43} & c_{44} & c_{45} & c_{46} \\ c_{51} & c_{52} & c_{53} & c_{54} & c_{55} & c_{56} \\ c_{61} & c_{62} & c_{63} & c_{64} & c_{65} & c_{66} \end{bmatrix} \cdot \begin{pmatrix} \varepsilon_{11} \\ \varepsilon_{22} \\ \varepsilon_{33} \\ \varepsilon_{12} \\ \varepsilon_{13} \\ \varepsilon_{23} \end{pmatrix} \tag{2.10}$$

The preceding stiffness matrix holds 36 values; however, some observations permit extensive simplification of this matrix. Most materials possess an interesting function called strain energy density. Related to the conservatism of a material, existence of strain energy density demands symmetry of the stiffness matrix. This symmetry indicates that only 21 of these 36 values are independent. Such is the case for an anisotropic substance (a material

without any planes of symmetry). It must be represented with 21 quantities obtained through experimentation (Cowin, Mechanics of Materials; Boresi and Chong).

$$\begin{pmatrix}\sigma_{11}\\ \sigma_{22}\\ \sigma_{33}\\ \sigma_{12}\\ \sigma_{13}\\ \sigma_{23}\end{pmatrix} = \begin{bmatrix} c_{11} & c_{12} & c_{13} & 0 & 0 & 0\\ c_{21} & c_{22} & c_{23} & 0 & 0 & 0\\ c_{31} & c_{32} & c_{33} & 0 & 0 & 0\\ 0 & 0 & 0 & c_{44} & 0 & 0\\ 0 & 0 & 0 & 0 & c_{55} & 0\\ 0 & 0 & 0 & 0 & 0 & c_{66}\end{bmatrix} \cdot \begin{pmatrix}\varepsilon_{11}\\ \varepsilon_{22}\\ \varepsilon_{33}\\ \varepsilon_{12}\\ \varepsilon_{13}\\ \varepsilon_{23}\end{pmatrix} \qquad 2.11$$

We can further reduce the necessary stiffness components by making additional observations about materials. Most materials exhibit independence between normal and shear behavior. This helps us populate our stiffness matrix with numerous zeroes such that only twelve values remain, nine of which are independent. Such a material is orthotropic and operates with 3 planes of symmetry. Wood is an example of an orthotropic material with unique properties depending on orientations of the wood grains (Cowin, Mechanics of Materials; J. L. Katz; Van Buskirk).

$$\begin{pmatrix}\sigma_{11}\\ \sigma_{22}\\ \sigma_{33}\\ \sigma_{12}\\ \sigma_{13}\\ \sigma_{23}\end{pmatrix} = \begin{bmatrix} \frac{1-\nu_{23}\cdot\nu_{32}}{E_2\cdot E_3\cdot\Theta} & \frac{\nu_{21}+\nu_{31}\cdot\nu_{23}}{E_2\cdot E_3\cdot\Theta} & \frac{\nu_{31}+\nu_{21}\cdot\nu_{32}}{E_2\cdot E_3\cdot\Theta} & 0 & 0 & 0\\ \frac{\nu_{12}+\nu_{13}\cdot\nu_{32}}{E_1\cdot E_3\cdot\Theta} & \frac{1-\nu_{31}\cdot\nu_{13}}{E_1\cdot E_3\cdot\Theta} & \frac{\nu_{32}+\nu_{31}\cdot\nu_{12}}{E_1\cdot E_3\cdot\Theta} & 0 & 0 & 0\\ \frac{\nu_{13}+\nu_{12}\cdot\nu_{23}}{E_2\cdot E_1\cdot\Theta} & \frac{\nu_{23}+\nu_{13}\cdot\nu_{21}}{E_2\cdot E_1\cdot\Theta} & \frac{1-\nu_{12}\cdot\nu_{21}}{E_2\cdot E_1\cdot\Theta} & 0 & 0 & 0\\ 0 & 0 & 0 & 2\cdot G_{12} & 0 & 0\\ 0 & 0 & 0 & 0 & 2\cdot G_{13} & 0\\ 0 & 0 & 0 & 0 & 0 & 2\cdot G_{23}\end{bmatrix} \cdot \begin{pmatrix}\varepsilon_{11}\\ \varepsilon_{22}\\ \varepsilon_{33}\\ \varepsilon_{12}\\ \varepsilon_{13}\\ \varepsilon_{23}\end{pmatrix} \qquad 2.12$$

$$\Theta = \frac{1 - \nu_{12} \cdot \nu_{21} - \nu_{23} \cdot \nu_{32} - \nu_{31} \cdot \nu_{13} - 2 \cdot \nu_{12} \cdot \nu_{23} \cdot \nu_{31}}{E_1 \cdot E_2 \cdot E_3} \qquad 2.13$$

The independent stiffness quantities reduce further to just five numbers if two of the orthogonal planes behave similarly. This is called transverse isotropy. An example of this would be concrete reinforced by steel rods aligned in one direction. The stiffness of the material along the rods would be unique compared to the two perpendicular directions (Beer; J. L. Katz).

The term "isotropic" refers to the most uncomplicated material behavior, in which any directs are equivalent, and behavior can be fully understood with a pair of material properties: elastic modulus and Poisson's ratio. Most metals behave isotropically. For this case, $E_1 = E_2 = E_3$ and all Poisson's ratios are equivalent and the shear moduli, G, are equivalent and dependent upon the modulus of elasticity and Poisson's ratio (Beer).

2.7 Compatibility

When considering interface boundaries between two materials, it is vital to understand the concept of compatibility and its influence on stresses, strains, and displacements. Previously, linear deformation has been operated upon to produce 6 strain quantities. We may now consider the connections between these six quantities and whether they can be arbitrarily selected and solved for deformations.

2.7.1 Introduction to Compatibility

Compatibility is an expression of constraint. Since there are only three displacements (u, v, w) but six equations for strain, the strain equations cannot be completely independent. It is therefore possible to correlate strain with additional relationships. The following six equations must be satisfied for small deformations in a 3D body. In two dimensions, a single equation is sufficient to describe necessary strain connections (Boresi and Chong).

$$\begin{aligned}
&\frac{\partial^2 \varepsilon_{xx}}{\partial y^2}+\frac{\partial^2 \varepsilon_{yy}}{\partial x^2}=2\cdot\frac{\partial^2 \varepsilon_{xy}}{\partial x\partial y} \qquad \frac{\partial^2 \varepsilon_{xx}}{\partial y\partial z}=\frac{\partial}{\partial x}\left(\frac{-\partial \varepsilon_{yz}}{\partial x}+\frac{\partial \varepsilon_{zx}}{\partial y}+\frac{\partial \varepsilon_{xy}}{\partial z}\right)\\
&\frac{\partial^2 \varepsilon_{yy}}{\partial z^2}+\frac{\partial^2 \varepsilon_{zzy}}{\partial y^2}=2\cdot\frac{\partial^2 \varepsilon_{yz}}{\partial z\partial y} \qquad \frac{\partial^2 \varepsilon_{yy}}{\partial x\partial z}=\frac{\partial}{\partial y}\left(\frac{\partial \varepsilon_{yz}}{\partial x}-\frac{\partial \varepsilon_{zx}}{\partial y}+\frac{\partial \varepsilon_{xy}}{\partial z}\right)\\
&\frac{\partial^2 \varepsilon_{zz}}{\partial x^2}+\frac{\partial^2 \varepsilon_{xx}}{\partial z^2}=2\cdot\frac{\partial^2 \varepsilon_{zx}}{\partial x\partial z} \qquad \frac{\partial^2 \varepsilon_{zz}}{\partial y\partial x}=\frac{\partial}{\partial z}\left(\frac{\partial \varepsilon_{yz}}{\partial x}+\frac{\partial \varepsilon_{zx}}{\partial y}-\frac{\partial \varepsilon_{xy}}{\partial z}\right)
\end{aligned} \tag{2.14}$$

$$\frac{\partial^2 \varepsilon_{xx}}{\partial y^2}+\frac{\partial^2 \varepsilon_{yy}}{\partial x^2}=2\cdot\frac{\partial^2 \varepsilon_{xy}}{\partial x\partial y} \tag{2.15}$$

The practical consequence of compatibility is such that some stresses cross a boundary of differing materials and some strains cross the boundary. When material properties differ, both stresses and strains cannot remain constant across a boundary. The enforcement of displacements and surface stresses at a boundary is sometimes known as mixed elastostatic boundary value problem (Cowin, Mechanics of Materials).

$$\begin{array}{lll} \overline{\overline{\sigma_N}} = \sigma_N & \overline{\overline{\tau_{Nt}}} = \tau_{Nt} & \overline{\overline{\varepsilon_t}} = \varepsilon_t \\ \overline{\overline{\sigma_s}} \neq \sigma_s & \overline{\overline{\gamma_{Nt}}} \neq \gamma_{Nt} & \overline{\overline{\varepsilon_N}} \neq \varepsilon_N \end{array} \qquad 2.16$$

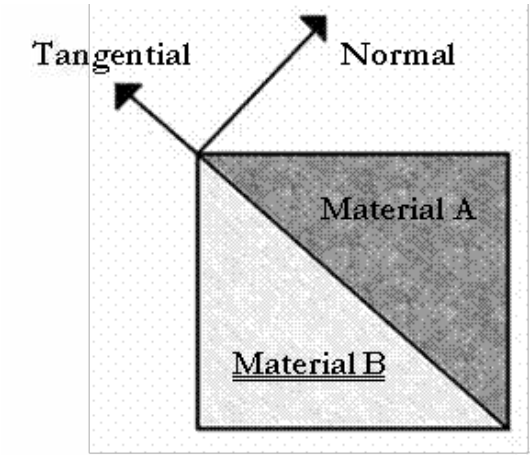

Figure 21. Two materials joined at a tangential surface

For enforcing compatibility along the boundary of two differing materials, we need only require that displacement along that boundary be consistent across the boundary. Each point along the boundary is bound to its partner from material to material. Due to differing material properties, this means that some stresses and some strains transfer across the boundary while others do not. This mathematical statement leads to very pertinent physical consequences by enforcing continuous deformations throughout the system and eliminating discontinuities.

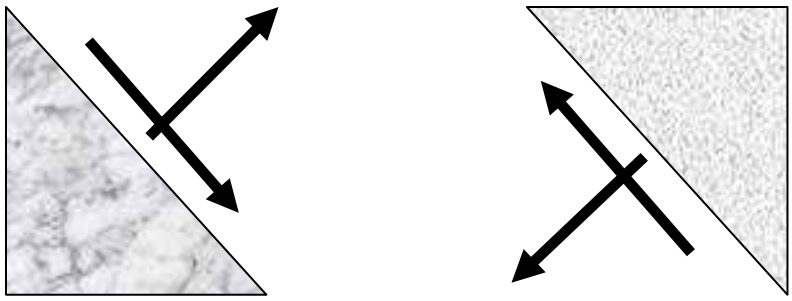

Figure 22. Separated composite structure showing equivalent traction

2.7.2 Axial Loading Compatibility

For an axially loaded rod, obtaining stress and strain is an easy task when the rod is of uniform material and well defined geometry. If some of this rod were replaced by new material (as in an implant), the original behavior should be preserved as best as possible.

$$\varepsilon_{axial} = \frac{P}{A \cdot E} \quad \Rightarrow \quad \sigma_{axial} = \frac{P}{A} \tag{2.17}$$

If half the height of the material were replaced, each portion would be expected to endure half of the load. Equivalent load and equivalent strain due to rigid bonding necessitates equivalent bulk stiffness (AE in this case). Any material of greater material stiffness would need a modified geometry to reduce its useful area (Bundy, Composite Material Models for Bone).

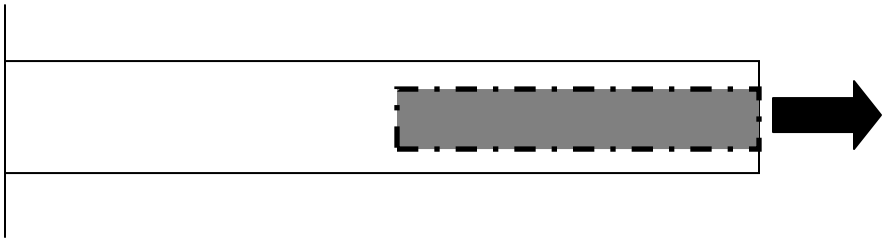

Figure 23. Axially loaded rod with segment substituted by alternative material

$$P = \left(A \cdot E\right) \cdot \varepsilon_{axial} \tag{2.18}$$

$$\left(A_a \cdot E_a\right) = \left(A_b \cdot E_b\right) \tag{2.19}$$

$$\left(\frac{A_a}{A_b}\right) = \left(\frac{E_b}{E_a}\right) \tag{2.20}$$

2.7.3 Bending Compatibility

Pure bending of a cantilever beam is also a well-understood and easily described scenario. In this situation, maintaining equivalent strains across the boundary requires adjustment, not of area, but of the 2nd moment of area. Because 2nd moment of area is 4th order with linear dimensions, even the slightest difference in stiffness translates into enormous differences in cross section, more so than in the axial loading case.

$$\varepsilon_{axial} = \frac{M \cdot y}{I \cdot E} \tag{2.21}$$

$$\left(\frac{I_{a/NA}}{I_{b/NA}}\right)=\left(\frac{E_b}{E_a}\right) \tag{2.22}$$

2.7.4 General Plane Stress Compatibility

A general loading problem can produce very complex relationships for bulk stiffness across boundaries. Location of the implanted material and nature of the various loads make prediction of the required geometry manipulation extremely difficult without a more intricate method of analysis.

2.8 Finite Element Method

When faced with a simple geometric structure under loading, the behavior of the structure can be determined to high accuracy with sufficient knowledge of solid mechanics. Whether a pressure vessel, cantilever beam, circular rod or shaft, or other fundamental structure lacking excessive geometric or material complexity; well-understood equations describe stress, strain, and displacement continuously within the structure. More complex systems require another approach.

The finite element method is a mathematical analysis technique by which we divide our solid structure into limited geometric structures, or “finite elements”. Each element possesses nodes, and we strive to describe a relationship between the interconnected nodes of a specific element by knowing its material stiffness and geometry. Once each element is fully described, an algebraic expression can be created which assembles the parts into an entire system. The method must maintain appropriate continuity of particular quantities across

nodes and elements so that we can obtain a highly accurate description of behavior for the complete structure or for specific local regions. Even though the general solution provides deflections just for the nodes, by using interpolation functions, any other interior coordinate point can be evaluated as well (Reddy; Hart, The Finite Element Method).

The system domain must be discretized, or divided, into a finite number of geometries known as elements. The elements can often take the form of a triangle, trapezoid, or rectangle, but may take any shape so long as an appropriate description of properties can be applied to relate the geometry. The number of nodes and elements is always a delicate balancing act between accuracy and complexity.

Consider an element whose points, or nodes, each have undergone displacement. These movements can be expressed with a simple vector where u, v, and w represent displacements in three dimensions for the various nodes of the element. The size of this vector depends on the number of nodes and the degrees of freedom (two for plane motion).

$$d^{T}_{element} = \{u_1 \quad v_1 \quad w_1 \quad u_2 \quad v_2 \quad w_2 \quad \dots \quad \dots \quad \dots\} \qquad 2.23$$

For plane problems, a triangular element is often convenient. Just about any two-dimensional shape can be satisfactorily approximated by many connected triangles (Hart, The Finite Element Method). Each triangle element is composed of three nodes, and because each node can move in the x and y directions, six displacement values define the entire element solution. It is then possible to define an interpolation function to describe interior node deflections. By assuming that deflections vary linearly within an element, a simple equation

requires only three coefficients, and these three coefficients are dependent upon the nodal displacement values (Reddy).

$$\begin{aligned} u_1 &= a_1 + a_2 \cdot x_1 + a_3 \cdot y_1 \\ u_2 &= a_1 + a_2 \cdot x_2 + a_3 \cdot y_2 \\ u_3 &= a_1 + a_2 \cdot x_3 + a_3 \cdot y_3 \end{aligned} \tag{2.24}$$

By using displacement for each of the three nodes, substitution allows us to evaluate the coefficients of the interpolation function. Keep in mind that this interpolation function defines deflection in the x-direction. A similar function can be defined for the y-direction.

$$\begin{Bmatrix} u_1 \\ u_2 \\ u_3 \end{Bmatrix} = \begin{bmatrix} 1 & x_1 & y_1 \\ 1 & x_2 & y_2 \\ 1 & x_3 & y_3 \end{bmatrix} \cdot \begin{Bmatrix} a_1 \\ a_2 \\ a_3 \end{Bmatrix} \qquad \begin{Bmatrix} a_1 \\ a_2 \\ a_3 \end{Bmatrix} = \begin{bmatrix} 1 & x_1 & y_1 \\ 1 & x_2 & y_2 \\ 1 & x_3 & y_3 \end{bmatrix}^{-1} \cdot \begin{Bmatrix} u_1 \\ u_2 \\ u_3 \end{Bmatrix} \tag{2.25}$$

With the coefficients determined, the interpolation functions can be rewritten to relate to the nodal displacements. In this form, the coefficients (indicated as "N") are known as shape functions and vary with the node coordinates and internal point coordinates.

$$u_x(x, y) = N_1(x, y) \cdot u_1 + N_2(x, y) \cdot u_2 + N_3(x, y) \cdot u_3 \tag{2.26}$$

$$\begin{aligned} N_1 &= \frac{1}{2 \cdot A} \cdot \left[(x_2 \cdot y_3 - x_3 \cdot y_2) + (y_2 - y_3) \cdot x + (x_3 - x_2) \cdot y \right] \\ N_2 &= \frac{1}{2 \cdot A} \cdot \left[(x_3 \cdot y_1 - x_1 \cdot y_3) + (y_3 - y_1) \cdot x + (x_1 - x_3) \cdot y \right] \\ N_3 &= \frac{1}{2 \cdot A} \cdot \left[(x_1 \cdot y_2 - x_2 \cdot y_1) + (y_1 - y_2) \cdot x + (x_2 - x_1) \cdot y \right] \end{aligned} \tag{2.27}$$

$$A = Area = \frac{1}{2} \cdot \det \begin{bmatrix} 1 & x_1 & y_1 \\ 1 & x_2 & y_2 \\ 1 & x_3 & y_3 \end{bmatrix} \tag{2.28}$$

Be expressing the deflections of any point within an element, it is now possible to evaluate strains. For plane problems, there are three relevant strains and each is obtained from a partial derivative of deflections. Note that the two deflection equations can produce three strain terms (Reddy).

$$\begin{Bmatrix} u_x \\ u_y \end{Bmatrix} = \begin{bmatrix} N_1 & 0 & N_2 & 0 & N_3 & 0 \\ 0 & N_1 & 0 & N_2 & 0 & N_3 \end{bmatrix} \cdot \begin{Bmatrix} u_1 \\ v_1 \\ u_2 \\ v_2 \\ u_3 \\ v_3 \end{Bmatrix} \tag{2.29}$$

$$\begin{Bmatrix} \varepsilon_{xx} \\ \varepsilon_{yy} \\ \gamma_{xy} \end{Bmatrix} = \begin{Bmatrix} \frac{\partial u_x}{\partial x} \\ \frac{\partial u_y}{\partial y} \\ \frac{\partial u_x}{\partial y} + \frac{\partial u_y}{\partial x} \end{Bmatrix} = \begin{bmatrix} \frac{\partial N_1}{\partial x} & 0 & \frac{\partial N_1}{\partial x} & 0 & \frac{\partial N_3}{\partial x} & 0 \\ 0 & \frac{\partial N_1}{\partial y} & 0 & \frac{\partial N_2}{\partial y} & 0 & \frac{\partial N_3}{\partial y} \\ \frac{\partial N_1}{\partial y} & \frac{\partial N_1}{\partial x} & \frac{\partial N_2}{\partial y} & \frac{\partial N_2}{\partial x} & \frac{\partial N_3}{\partial y} & \frac{\partial N_3}{\partial x} \end{bmatrix} \cdot \begin{Bmatrix} u_1 \\ v_1 \\ u_2 \\ v_2 \\ u_3 \\ v_3 \end{Bmatrix} \tag{2.30}$$

$$\varepsilon = B \cdot d \tag{2.31}$$

$$B = \frac{1}{2 \cdot A} \cdot \begin{bmatrix} y_2 - y_3 & 0 & y_3 - y_1 & 0 & y_1 - y_2 & 0 \\ 0 & x_3 - x_2 & 0 & x_1 - x_3 & 0 & x_2 - x_1 \\ x_3 - x_2 & y_2 - y_3 & x_1 - x_3 & y_3 - y_1 & x_2 - x_1 & y_1 - y_2 \end{bmatrix} \tag{2.32}$$

$$\sigma = D \cdot \varepsilon = D \cdot B \cdot d \tag{2.33}$$

The strain/displacement matrix, B, is constant for these elements just as the stiffness matrix, D (which is often expressed as E, S in other problems). These equations are now extremely useful in applying our finite element model. This is a direct consequence of our assumed linear shape function inside the triangular element (Reddy).

It is now useful to discuss energy stored in a distorted element. In much the same way we can evaluate energy stored in a spring, a two-dimensional element can store energy, and this is often expressed in terms of strain and stress. In the energy equation shown, V is the volume of the element (or area times thickness). Because we have other expressions for stress and strain, this energy can then be rewritten as in equations 2.34 and 2.35 (Reddy).

$$Energy = \frac{1}{2} \cdot \varepsilon^T \cdot \sigma \cdot V \tag{2.34}$$

$$Energy = \frac{1}{2} \cdot d^T \cdot B^T \cdot D \cdot B \cdot d \cdot V \tag{2.35}$$

$$Energy = \frac{1}{2} \cdot d^T \cdot \left(B^T \cdot D \cdot B \cdot V\right) \cdot d \tag{2.36}$$

The overall stiffness, K, and deflection provide this energy for any element. This stiffness depends on the material and geometric properties of the element, including the material stiffness, the area, and the thickness (Hart, The Finite Element Method).

$$Energy = \frac{1}{2} d^T \cdot K \cdot d \qquad K = B^T \cdot D \cdot B \cdot A \cdot t \qquad 2.37$$

For each individual element, the stiffness, K, can be evaluated. These components of stiffness can then be summed to obtain a global stiffness for the system. Just as in springs, With the stiffness and applied forces known, deflection can easily be calculated.

2.9 Bone Properties

While the mechanisms for bone resorption and deposition discussed earlier are certainly interesting, the significance of this has not yet been fully discussed. Activity of the osteoblasts, osteoclasts, and osteocytes does not replace bone identically to the previous bone configuration. Slight variations result from generation to generation. This produces adaptation; and this is generally a positive effect which results in a type of operational efficiency (Jee).

Any comparison of the bones of children and adults reveals significant differences. While young bones are more random in their orientation of bone layers, older bone begins to show greater alignment in predictable orientations. The daily usage of the bone influences the operation of osteoblasts, osteoclasts, and osteocytes to improve typical bone performance (Charnley; Rhoades). In a sense, the individual bone components working to their own directives create a distinct global directive. The bone seems to learn how to make the most of the limited material available. Such improvements in performance lead properties of the bone to diverge for unlike directions. It is for this reason that bone is best treated as not simply

isotropic for behavioral analysis. The following sections further analyze these properties of bone (Jee).

2.9.1 Cortical Bone Properties

There is significant disagreement among researchers in defining properties of bone. To a large degree, this is unavoidable. Variations in gender, age, lifestyle, type of bone, and numerous other factors produce vast differences. Additional incongruities may exist due to differing testing methods or behavioral models (Cowin, The Mechanical Properties of Cortical Bone Tissue; Van Buskirk).

Cowin (The Mechanical Properties of Cortical Bone Tissue) in 1989 discusses that many researchers model cortical bone as transversely isotropic or orthotropic. The data presented varies greatly, partly because a portion of bones for analysis came from cow bones. When researchers did model bone as orthotropic, there was obvious similarity between the non-axial load stiffnesses. It is for this reason that so many analysts view bone as transversely isotropic.

Fung (Biomechanics: Mechanical Properties of Living Tissues) discusses various properties of cortical bone and the great disparity between sources citing them. Some cited sources present an isotropic modulus of elasticity in tension of 17.6GPa. Others model dense bone as transversely isotropic with the two key moduli being 17GPa and 11.5GPa in axial and transverse orientations, respectively.

Using nanoindentation in 2005, Silva (Elasticity and Viscoelasticity of Human Tibial Cortical Bone Measured by Nanoindentation) evaluated the elastic modulus of wet cortical

bone at approximately 15GPa. This data was obtained for the human tibia, however, so we cannot guarantee consistency to other bones of the body.

Van Burstein and Reilly (The Elastic Moduli of Bone) presented extensive data showing variation circumferentially and along the length of the femur. Little exists in the literature to corroborate this presentation of data and much more trustworthy seems the authors' own transversely isotropic properties that have been so often used by other authors.

2.9.2 Cancellous Bone Properties

As with cortical bone, cancellous bone has been shown to express properties over an enormous range. Such wide variation is a consequence of extreme variations in usage, age, genetics, and additional properties. Cancellous bone is of lower density than cortical bone, but is more susceptible to adaptation over time. Oftentimes, cancellous bone stiffness is modeled as a function of density (Cowin, The Mechanical Properties of Cancellous Bone).

When Cowin (Cowin, The Mechanical Properties of Cancellous Bone) presented a summary of elastic moduli, as always, the isotropic values maxed at 20GPa. This value seems unexpectedly high for spongy bone. All in all, selecting trustworthy data from this assortment is difficult.

Goldstein (The Mechanical Properties of Trabecular Bone: Dependence on Anatomic Location and Function) presents a summary of many analyses which illustrate the vast disparity in properties. For the various sources presented here, the modulus of elasticity ranged 7.6MPa to 9800MPa. Little can be conclusively derived from this beyond the

observations that cancellous bone tends to possess stiffness approximately one-third that of cortical bone.

Because properties in the literature vary so greatly, selecting appropriate will always be a challenge. Most significant seems the necessity of varying cancellous bone strength along the femur and providing complexity at least as significant as transverse isotropy. Furthermore, typical densities of bone tissue indicate that the stiffness or cancellous bone would generally range 5%-40% that of cortical bone.

2.9.3 Bone Adaptation & Wolff's Law

In 1867, G.H. Meyer published "Die Architektur der Spongiosa." Meyer had observed what many others had regarding consistent interior features of various bones. Meyer presented diagrams of the interior of bones showing structurally significant orientations. A mathematician named C. Culmann believed that principal stress trajectories matched the bone drawings that Meyer presented. These early observations and meetings of minds initiated some important trains of thought regarding notions of bone adaptation to match loading conditions (Roesler; Cowin, The False Premise in Wolff's Law).

A German surgeon named Julius Wolff (b. 1836) took notice of these prior analyses and, from 1869 onward, published extensively on the subject of bone adaptation. Wolff developed a law of bone transformation which has since earned the name "Wolff's Law" (Fung; Huiskes). This law held, among other things, that cancellous bone growth entirely corresponded to trajectories of principal stresses presented by Culmann in a series of drawings known as the Culmann crane (Roesler; Cowin, The False Premise in Wolff's Law).

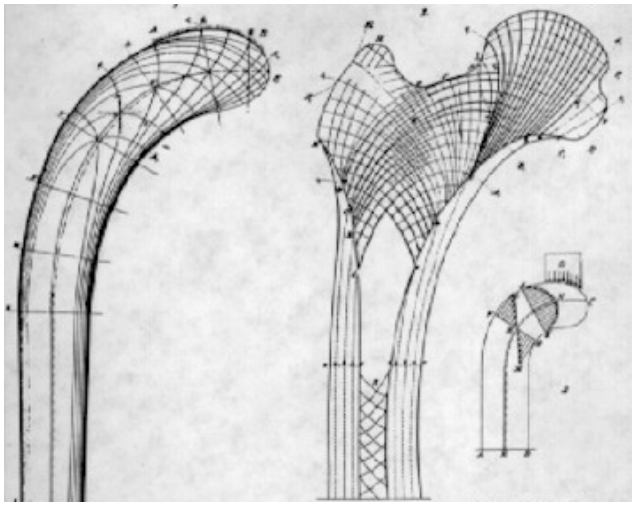

Figure 24. Culmann crane diagrams

Certain aspects of Wolff's analyses have come under criticism over the years. The Culmann drawings themselves are questionable as an accurate representation of stress trajectories for a specific load. Wolff, in using Culmann's crane drawings, makes several statements which seem to indicate lack of thorough understanding of the relevant mathematical relationships while he makes additional incorrect assertions about bone behavior. Furthermore, Wolff's decisive declarations lack rigorous mathematical backing to justify being called "proof" as he states (Pearson; Roesler; Cowin, The False Premise in Wolff's Law).

Regardless of questions regarding Wolff's methods of analysis, it is widely accepted that bone does adapt itself in response to regular loading (Rhoades). Bone is more significantly deposited in sites subjected to larger stresses and is resorbed from sites where there is little stress. This apposition, due to the diligent operation of bone cells, produces the commonly observed trajectories in cancellous bone tissue (often called trabecular bone) and

leads to greater strength of bone in the most commonly used modes. It is this very beneficial process which eventually turns unfavorable in the presence of a typical hip implant – a detrimental process named stress shielding (Cowin, The False Premise in Wolff's Law).

In 1987, Wuh (Strain Analysis of the Proximal Femur After Total Hip Replacement) showed how strains distort for many locations for multiple downward loads. Strains reduced for medial, proximal points while increasing for lateral, proximal points. The vast majority of points loss average magnitude of strain. Therefore, bone could build up in some places while diminishing on the other. Larger loads enhanced all effects.

2.9.4 Variation of Properties

Bone, as an imperfect distribution of organic and inorganic parts, possesses variation of properties from region to region – not only between cortical bone and cancellous bone but within each type of bone as well. Naturally, density in any given bone region greatly affects properties in that region, making bone heterogeneous. In addition, the distribution of bone cells, collagen, impurities, and bone minerals produces a complex directional behavior. The longitudinal strength will differ from transverse strength in significant ways. This anisotropy has been often demonstrated through material testing of bone even though many experiments show that orthotropic behavior is sometimes an acceptable model. Modeling as orthotropic is sometimes a worthwhile simplification to analysis (Van Buskirk).

2.9.5 Viscoelasticity

All biological materials possess some level of viscoelasticy – a property indicating time-dependent relationships between stresses and strains. Bone, when experimentally loaded over a long period of time, will continue to stretch rather than reach some instant equilibrium as a theoretical massless mechanical spring might (Fung; L. d. Silva). The viscosity of bone was discussed in (Cowin, The Mechanical Properties of Cortical Bone Tissue) and illustrated as significant at high speeds, yet few effects would manifest at a typical walking pace. This effect is usually considered negligible for many purposes and will not be examined in this study.

2.10 Implant History

Through numerous developments, the modern day total hip replacement was born under the direction of John Charnley in the late 1950s and early 1960s (Bundy, Bone Prosthesis and Implants; Hungerford). He attempted using various materials in all parts of the hip joint (including Teflon which proved insufficient to articulate with metal). Eventually, his early successful innovation utilized 3 important materials: stainless steel for the femoral head, polyethylene for the acetabular socket, and polymethylmethacrylate (PMMA) for fixation of both components. While the polyethylene provides smooth pain-free sliding with the steel, the stainless steel is biocompatible, resists moisture, and provides great strength in all modes of activity. The PMMA is a bone cement that has commonly been used in dentistry for its beneficial properties. The strength of PMMA lies between that of cortical bone and cancellous bone, a benefit to reducing bone resorption (Charnley).

Charnley's low friction arthroplasty has been successfully used since its inception, forever linking his name to these procedures. Incremental changes in materials and procedures since the 1960s allow greater comfort or longevity of the implant while largely maintaining Charnley's arrangement. Few full hip replacements use alternatives to polyethylene for the acetabulum; however, some implants comprise cobalt-chrome or titanium alloys rather than stainless steel. Such changes may result from variations in cost, availability, or desired implant stiffness or strength. There are some reports that younger patients have less success with Charnley systems (Joshi).

One particular deviation from the Charnley system results from realizations that some patients experience great success without using bone cement for the femoral component. In some cases, it was found that natural bone growth to the implant can provide sufficient support, but this system requires that the implant must fit more securely at the completion of surgery. Bone immediately begins growing around the implant, and after sufficient time has passed, the patient can bear a load. Some debate exists over appropriate circumstances to use cemented versus non-cemented implants, yet it is largely a matter of the patient's age. Older patients tend to be given cement in order to allow almost immediate ambulation while younger patients have more success without cement.

Serbousek (Reduced Stiffness Femoral Hip Implant) obtained a patent in 1994 for an implant of reduced stiffness. While the stem does substantially fill the medullary canal, a groove extends along much of the length of the medial edge of the stem in order to reduce stiffness. Further components include a collar at the shoulder for better transmission of normal forces and a surface coating for encouraging bone ingrowth fixation.

Rather than improving geometry, Kuiper and Huiskes (Mathematical Optimization of Elastic Properties: Application to Cementless Hip Stem Design) focused their optimization efforts on changing the material properties of a potential hip stem. They note that stiff stems shield the bone from normal stress states while flexible stems lead to high interface stresses which can also lead to failure. This 2D analysis utilizes a pure bending moment and models the bone as isotropic. The solution is a field of moduli for the implant. Most of the shown solutions possessed much lower stiffnesses distally furthering the concept of short stems often being superior for reduction of stress shielding. Additionally, it was found that some underloading is tolerated by bone.

Evans (Numerical optimization of the design of a coated, cementless hip prosthesis) conducted a 1D finite element analysis (within ANSYS) by using beam elements to describe bone and implant. The solid implant had variable exterior geometry described by nine parameters which optimized to reduce stress shielding and interface stresses. The resulting design shows clear improvement over initial values as stresses within the bone were transmitted in a far more favorable way. The implant was modeled as Ti-6Al-4V and all the bone and implant materials were modeled as isotropic. The loading more closely matched standing conditions even though the authors acknowledge that walking or running loads might provide more appropriate solutions.

Rahman (Stem Stiffness Optimization and Material Properties Evaluation of the Hip Prosthesis) used the same titanium alloy as Evans for an implant and compared with two other possible implant materials: cobalt-chrome alloy and CFRP composite. The axisymmetric finite element models were fit to stair climbing loads and then optimized internally such that

the interface of implant and bone was fixed. As expected, stiffness of the implant greatly influences resulting interface stresses. The researchers concluded that lower implant stiffness distally reduces stress shielding in the nearby bone.

Natarajan (A Relationship Between Stress Shielding and Stem Stiffness in the Proximal Femur After Total Hip Replacement) carried out a 3D finite element analysis of various materials in a fixed implant to determine their effects on the resulting bone stresses. This parametric study compared cobalt-chrome, titanium, and two composite materials. In this manner, the stresses were compared to determine, not just rank of stresses, but also the degree to which stiffness influences changes in stresses. The more distal regions of bone were very resistant to stress changes due to stiffness of the implant. The proximal bone maintained very high sensitivity to stiffness but a major reduction in stiffness was necessary to bring stresses toward normal performance levels. Bear in mind the proximal bone acquired lower stresses than normal. This is equivalent to higher stress shielding.

Simões (Preliminary investigation of a novel controlled stiffness proximal femoral prosthesis) designed an implant with cobalt-chromium core and flexible composite outer layer. All materials were assumed isotropic, and the composite layer thickness was optimized by examining von Mises stresses at the interface. Research indicates that a stiff proximal implant and flexible distal implant produce the ideal stress state.

In 1997, Thongpreda (Implant Fixation System) obtained a patent with another method of reducing stiffness. A slot progresses from mid-stem to the distal edge. As always, the properties of this feature are meant to better match true bone behavior, but the implant

utilizes additional attributes. A commonly applied collar at the shoulder transmits axial loading, and a subtle, unique stem curvature allows for more ideal implantation.

Smith (Controlled Stiffness Femoral Hip Implant) produced an implant design with a much deeper channel along the medial stem. This more significantly reduces stem stiffness with the goal of better matching bone behavior. This patent submission even includes some basic analysis of solid and hollow implants but little is said about the use of hollow stems.

Cunningham (Hip implant prosthesis) produced an implant patent which attempted to remedy stress shielding effects. The design incorporated "load shoulders" in order to better transfer normal loads to the remaining bone structure. The implant shaft possessed a more slender diameter than the cortical/cancellous interface layer in addition to a distal bulge which would interface with the cortical bone layer. He supports this patent with supporting analysis showing reduction in stress shielding, however, this method greatly simplifies the bone geometry and behavior (Minimizing Stress Shielding in Hip Implant by Mechanical Design).

Katoozian (Three-Dimensional Shape Optimization of Femoral Component of Hip Prostheses with Nonlinear Frictional Interface) presented an optimization which focused on interface friction effects. This work carried out analysis of a cemented cobalt-chrome implant. Cortical bone was assumed isotropic (20GPa) and homogeneous. Cancellous bone was modeled as heterogeneous but isotropic – the modulus of elasticity ranged 1GPa to 5GPa. All materials utilized a poisson's ratio of 0.3. For this optimization, external geometry was varied to reduce friction interface effects.

Chang (Design and Analysis of Robust Total Joint Replacements: Finite Element Model Experiments with Environmental Variables) attempted to optimize a femoral implant

based on variation in a flexible midstem. This feature is defined by its location along the stem and its diameter which is substantially reduced from the rest of the implant diameter. Strain energy density was a key evaluating parameter of any design. The implant material was cobalt-chromium (220GPa modulus) and bone was allowed to vary somewhat with position. The final design possessed a very slender midstem (7mm diameter) but the distal edge of this midstem was deemed insignificant to the outcomes.

Joshi (Analysis of a femoral hip prosthesis designed to reduce stress shielding) used a short stem with a proximal plate and a cabling system to attempt to minimize stress shielding. Cortical bone properties were orthotropic and homogeneous while cancellous bone was isotropic but heterogeneous, both using very typical values. The implant was modeled as cobalt-chromium. The evaluation showed a definite improvement in the stress state of the remnant bone.

In 2001, Higa (Shape Optimization of Femoral Components of an Artificial Hip Prosthesis Using the Three-Dimensional P-Version Finite Element Method) used maximum principal stress to optimize four external implant design parameters. The three-dimensional analysis modeled all materials as isotropic. The bone tissues possessed moduli of 17GPa and 1GPa while cobalt-chromium's stiffness was 210GPa and bone cement 2.2GPa. The final design possessed a reduced implant width of the distal implant.

Mandell (A conical- collared intramedullary stem can improve stress transfer and limit micromotion) examined the properties of a conical collar to improve the stress state of a cylindrical bone-implant system. While many implants possess some flat segment at the shoulder of the implant, they are typically not conical. The implant was modeled as cobalt-

chromium while the bone was cortical, annular, and transversely isotropic with a large axial load. Properties came from Reilly and Burstein (as in many studies) for whom 17GPa was the axial modulus. Strain energy density, micromotion, and interface stresses determined the value of a given design. If a flat collar has a 0 degree angle, the ideal angle range for the collar was 30-60 degrees.

Pawlikowski (Process of hip joint prosthesis design including bone remodeling phenomenon) analyzed surgeon-directed implant designs of very unique construction. The somewhat amorphous structures (three of them) were each analyzed in a 3D finite element analysis in order to assess its stress shielding. A bone remodeling simulation allowed proper selection of the best design.

In 2006, Zakeri (Optimal Design of a Hip Joint Implant with Hollow Stem Using Finite Element Method) did attempt optimization of a 3D hollow cobalt-chromium stem. Von Mises stresses were used to evaluate a given design, and all materials were represented as isotropic. Cortical bone was given a modulus of elasticity of 20GPa while the modulus for cancellous bone varied along the length of the femur from 2GPa – 10GPa. It was observed that shorter stems tended to improve the stress state.

Such extensive and diverse research continues with the goal of reducing stress shielding further and further until, perhaps, its effects can be neglected. There are merits to each and every approach discussed here and we can learn a great deal from their progress. We can also formulate an original approach to contribute to this ongoing endeavor.

3. RESEARCH TOOLS

Matlab is a program useful for computing and programming. It provides a helpful environment for carrying out numerous technical operations such as plotting functions, matrix manipulations, and development of algorithms. Furthermore, Matlab possesses the capability to readily interface with other programs and file formats to act as a brain for complex operations and analyses. Therefore, we can open files, read files, search files, and write new files in various formats, all while carrying out lengthy algorithms which utilize the read information. Such control is a valued part of this research endeavor.

GMSH is a computer aided design (CAD) software for geometry description and visualization and mesh generation. With a given prescribed geometry, GMSH can generate an appropriate mesh useful in finite element modeling. Including this program in our optimization framework obviates the need for writing code to fully discretize the solid into abundant nodes. GMSH divides the solid appropriately and provides accessible output formats for reading the node locations.

Working in conjunction, these software will carry out all operations necessary to complete the geometry optimization.

4. RESEARCH METHODOLOGY

From the prior research, we must make numerous decisions in order to balance the desired accuracy for our results with sufficient simplicity for economical computational demands. The approach settled upon will be detailed in what follows.

4.1 Optimization Considerations

A common methodology for implant optimization involves merging of the implant model and bone model within finite element software. With appropriate cost functions defined – generally based on von Mises stresses within the bone at the bone/implant interface – the geometry or material properties of the implant are optimized through many iterative attempts to minimize cost. This finite element system requires extensive computational resources for the multiple bodies with differing material properties. Reducing the system complexity could greatly improve the optimization time; this is one goal of this work.

The current research additionally questions the use of von Mises stresses to analyze threat of stress shielding. Von Mises stresses are obtained from distortion energy of the point stresses, and while using this amalgamation of all stress components to produce a single value is quite successful in predicting material failure, it does not necessarily follow that stress shielding will respond most aptly to this parameter. Energy is a scalar value, lacking any directional component. Consider two points with nearly identical stress states, yet one is shifted 90° relative to the other: they would possess an identical Von Mises stress value even

though the orientation of the maximum stress, minimum stress, maximum shear stress, and others would be distinct.

We can infer from past research that the remodeling of bone by osteoblasts and osteoclasts with use produces organized lamellae precisely because orientations of the individual stress components within bone are entirely relevant to adaptation. It is preferable to consider contributions of each normal stress and shear stress so that individual stress contributions are not blurred.

In past research, focused on optimizing external implant geometry, an obstacle lies with the bone's dependence on implant geometry after implantation. As the implant improves through optimization, the bone must adjust to produces an entirely new bone/implant boundary. The new external boundary could lay more or less within the cancellous or cancellous bone layer – or perhaps even within the medullary cavity. Each intrusion of new material could produce a sudden synergistic jump in behavior.

Alternative researchers examine material properties of the implant, the goal being construction of a composite material with varying modulus of elasticity throughout for matching the overall bone behavior. In each case, the materials are coupled for analysis, a demanding computational concern. Furthermore, fabrication of an optimized implant with a specific heterogeneous stiffness field may prove quite a challenge.

The current research respects these past considerations in developing an innovative optimization framework. Whether slightly, somewhat, or very successful, it is hoped that past deficiencies can be diminished significantly with a less commonly considered approach: optimization of the internal implant geometry.

A material can be selected based on biocompatibility, surface roughness, and stiffness. External implant geometry can be fixed as well – prescribed by physicians for ideal implantation or by independent research on ideal external geometries. This means that bone/implant boundary is fixed while only the hollow interior varies with each iteration. The mode of optimization allows that the finite element models of the bone and implant be uncoupled and stress orientations preserved.

These goals are accomplished through enforcement of compatibility across the external implant surfaces, known as the "virtual boundary". The proposed Virtual Compatibility Optimization is enforced by prescribing deflections on the exterior implant surface: acquired from virtual boundary of the complete bone model. When the boundary stresses of the implant boundary produce normal and shear stress that are the same as in the pure bone condition, compatibility is enforced as if the implant and bone model were merged within one system. This condition constrains the bone/implant boundary such that stresses in the remaining bone are equal to a pure bone condition. Stress shielding could theoretically fall to zero in this circumstance.

Figure 25. Reversal of loads

Typical analyses of implants and bone begin with constraint of the distal femur while applying loads to the head and neck (as is anatomically appropriate). However, because the final analysis of this work (an implant constrained alone) contains no bone, it would not be possible to place constraints distally on nonexistent material. A simple solution lies in reversing the applied loads and reactions. In the initial, intact femur, the load conditions are altered such that the load points become constraints while the distal constraints become load points. Differences in the two surface locations and orientations necessitate transformation of load magnitudes to appropriate force/moment combinations. The net result should produce virtually identical internal behavior.

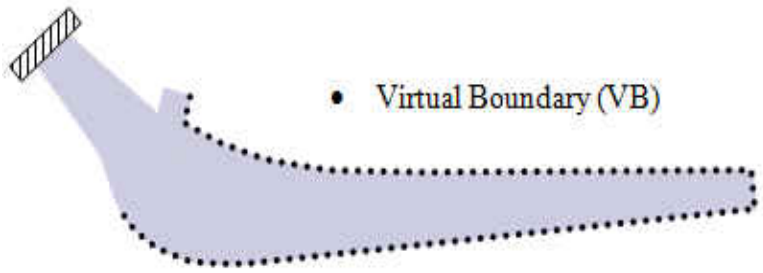

Figure 26. Implant constrained at the neck and showing the virtual boundary

After reversing loads, we can commence virtual implantation: the implant is aligned so that its shaft fits within the medullary canal, the transverse plate lies just proximal to the lesser trochanter, and the neck aligns within the boundaries of the now absent femoral neck. A section of bone must be removed to accomplish this task, but most of the greater trochanter and all of the lesser trochanter remain for muscle attachment.

Some care must be taken when using load reversal. If a loading surface is instead clamped, the constraint will not allow transverse displacement as could occur with a free

surface. Either the surface must be partially constrained to limit some, but not all, distortions or we must justify ignoring this effect.

Consider an axially loaded rod fully constrained at a wall. The free end can contract significantly as prescribed by modulus of elasticity and poisson's ratio within Hooke's Law. At the wall, vertical normal stresses develop to maintain zero strain. Were we to reverse constraint and loading, behavior at each end of the beam would diverge from the initial state. Conveniently, transverse stresses are generally significantly smaller than longitudinal stresses, and within the middle of the rod, there is greater agreement with the initial state. For these reasons, a long specimen (such as a femur) permits proximal and distal constraint while the virtual boundary to a relatively small degree.

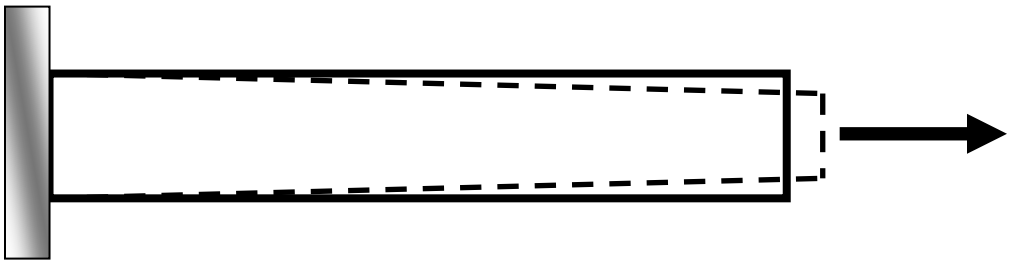

Figure 27. Notice that the wall constraint prevents transverse strain

When the intact femur is constrained and loaded, the goal is extraction of deflections along the virtual boundary as well as normal and shear traction along the virtual boundary. To this end, a partition must be generated within the bone. This partition corresponds to the desired position of the artificial implant (known as the virtual interface or virtual boundary) and should be chosen based on proper medical counsel. As each VB node passes through a bone element, the plane stresses (3 of them) are obtained and converted into normal and shear

traction (2 values). It is these 2 values that cross a composite boundary intact in order to enforce compatibility.

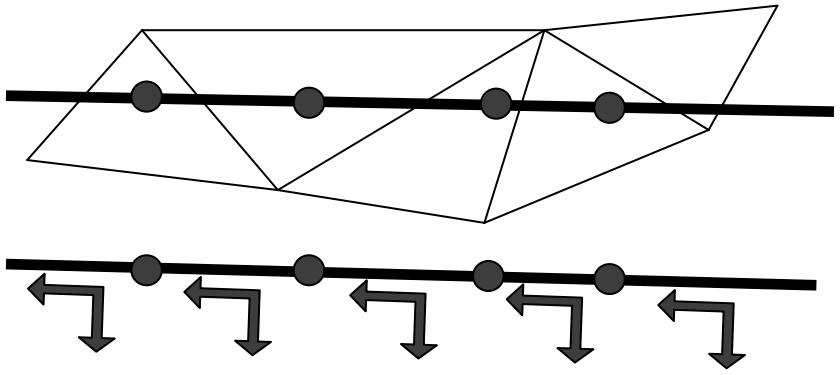

Figure 28. Virtual boundary passing through linear elements, for which we obtain traction along the surface

At this stage in the optimization process, the femur model is no longer necessary. We have acquired all necessary information from that intact bone analysis and this can now be utilized for our implant optimization – an optimization that does not require implantation. The internal geometry can now be optimized in a less computationally demanding process.

Based on our literature search, loading properties, material properties, and geometry properties were selected to best reflect true behavior and the goals set forth within this research. Each selection is detailed below.

4.1.1 Loading Conditions

The loading condition used here corresponds to a maximum loading during heel strike of a walking gait. At this point in a person's motion, the dominant loading occurs in the

coronal plane with a load of approximately three body weights at an angle between 10 and 15 degrees off axial toward the lateral side of the femur. The effect of this is to cause axial compression, bending, and transverse shear. While there are always muscles at work during motion, during this point in a walking gait, the muscle forces are smaller than the axial loading and will be neglected.

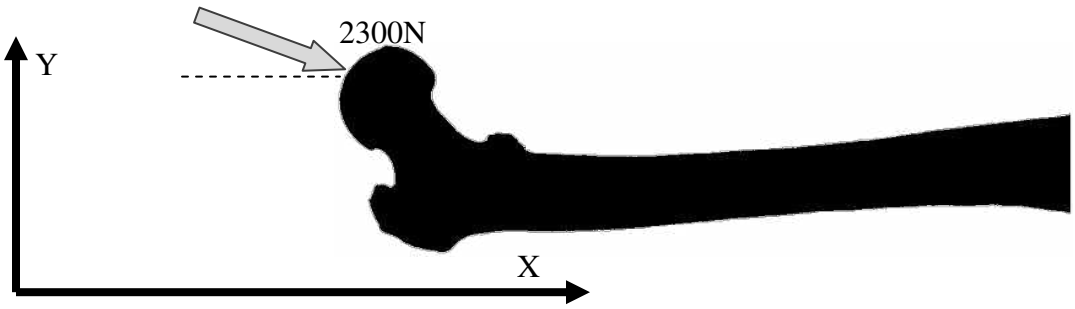

Figure 29. One load case showing approximately several body weights applied 15 degrees from axial

One load scenario utilizes a 2300N load applied 15 degrees from axial axial direction toward the lateral side of the femur. The second load case applies a 3000N load with an angle of 10 degrees. These two cases are both appropriate for heel strike during a normal low-speed walking gait. Muscle involvement is minimal and body weight is the dominant concern.

4.1.2 Cortical Bone Properties

While complex behavioral analysis is possible and has been done in the past, there is such great disagreement in appropriate orthotropic or anisotropic values that selecting appropriate conditions remains an enormous challenge. It is more generally accepted to treat

cortical bone as homogeneous as there is less variation in cortical bone density when compared to cancellous bone.

Cortical bone is certainly not isotropic and avoiding this characterization is a primary goal of this research. This leaves the option of characterizing cortical bone as transversely isotropic. While there is still great variation in some studies, we find sufficient agreement to select properties as shown here (Van Buskirk). All cortical bone elements within the original finite element bone model acquire these properties.

$$E_1 = 17GPa; \quad E_2 = E_3 = 11.5GPa \quad \upsilon_{12} = .46 \quad \upsilon_{31} = .31 \quad G_{13} = 3.28GPa \qquad 4.1$$

4.1.3 Cancellous Bone Properties

Much like the density of cancellous bone relative to cortical bone, the stiffness of cancellous bone generally ranges 5% to 40% of that of cortical bone. This spongy bone also possesses much greater heterogeneity. For this research, we assumed transversely isotropic behavior yet allowed properties to vary over the length of the femur. Over the length of the femur, three unique stiffness matrices were applied with the axial moduli progressing from 5GPa to 3GPa to 1GPa. The transverse moduli maintained the same ratio as in the cortical bone tissue. Poisson's ratios were kept the same as for cortical bone. Only 10cm from the most proximal edge, the cancellous bone ends within the medullary cavity. At this stage, only cortical bone remains.

The implant model possesses an identical neck design and is constrained identically to the bone model. Virtual interface deflections are applied to the appropriate exterior nodes. In

response, the constrained nodes resist deflection with reaction forces. These reaction forces are read into the algorithm for analysis. Each new design of the internal geometry will produce reaction forces closer or farther from the target reactions. The nature of the algorithm determines in what manner the geometry progresses.

4.1.4 Bone Geometry

A 2D image of a human femur, arranged in the coronal plane of loading, was utilized as a model for bone analysis. Forty centimeters of proximal femur were isolated as behavior in the distal knee joint is beyond the scope of this research. Furthermore, the implant lies well short of the terminal distal surface and will not be affected by end effects.

For the diaphysis, cortical wall thickness was made 30% of maximum width. Within the femoral head and neck, cortical thickness was fixed at 2mm. The rest of the femur transitions smoothly to bridge the gap between these differing thicknesses.

Figure 30. Forty cm of the proximal femur in the coronal plane used for FEA

4.1.5 Implant Properties

Our optimized implant is composed of a biocompatible titanium alloy: Ti-13Nb-13Zr. The moniker indicates 13% Niobium and 13% Zirconium. The combination of these elements in this particular alloy gives an approximate modulus of elasticity of 80GPa. Poisson's ratio is 0.32, and the yield stress is approximately 800 MPa. The lower modulus of elasticity more closely mimics bone stiffness than most other titanium allows. This selection makes optimization of the geometry easier since the larger the difference in stiffness, the thinner the implant walls necessary to permit adequate deflection and stresses.

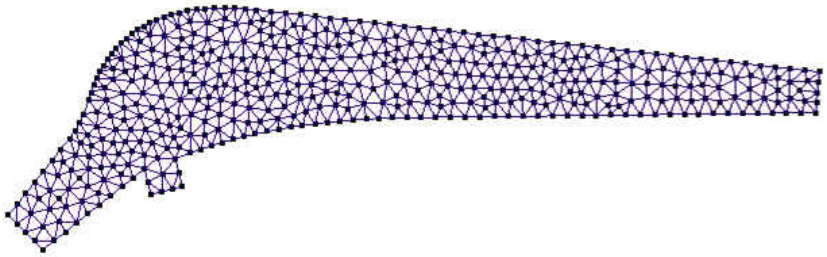

Figure 31. Solid implant design

4.2 Finite Element Analysis

All analyses utilized criteria for plane stress and linearly interpolated triangular elements. The limitation of this is that we have uniform stresses and strains within each element. Therefore, stress values are limited in accuracy, but with sufficient mesh density, very good stress and deflection responses can be achieved.

4.3 Optimization Conditions

The ten design parameters are limited by an upper and lower boundary. From the centerline inside the implant, the parameters define distance of each parameter. Parameters extend on either side of this centerline. They may not trespass too closely to the bone's outer surface nor may they encroach on the centerline. At five locations along the implant centerline, parameters extend to either side to help define the internal shape.

$$\text{Minimize } F(\sigma_j)$$
$$F(\sigma_j) = \sum\left(\sigma_j - \sigma_{target}\right)^2 + \sum\left(\tau_j - \tau_{target}\right)^2 \qquad 4.2$$
$$x_i^L \le x_i \le x_i^U$$

4.4 Algorithm of Optimization

The current problem presents some interesting challenges. While we do possess a fixed number of parameters, each parameter possesses a range of possible values rather than discrete values. Therefore, there is no finite combination of parameters. Depending on the number of divisions a person chooses within any range, we can produce tens of thousands to billions of combinations. For this reason, a brute-force algorithm is to be avoided.

An incremental approach has the detriment of potentially falling into a local minimum thereby failing to find a global minimum. A random search like the Monte Carlo Method may have the benefit of avoiding local minima and thereby finding a global minimum. At the same time, it is highly suspected that solutions may lie at the extreme upper or lower

boundaries. A random search may not find these particular extremes without some assistance. Therefore, randomness is incorporated but within a well-defined parameter space.

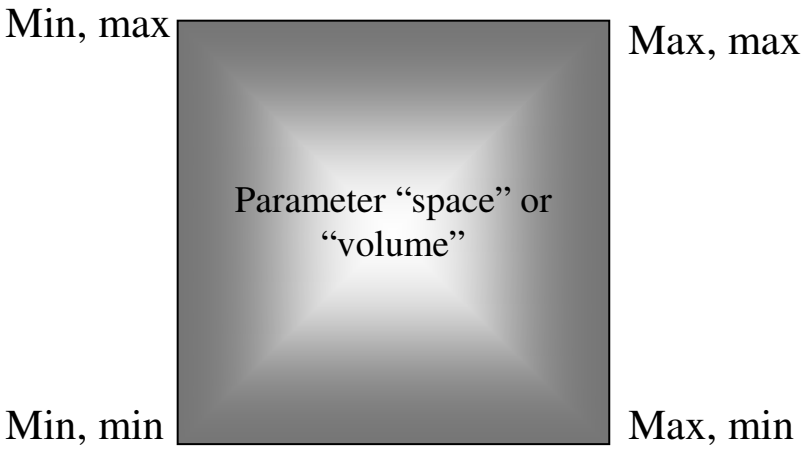

Figure 32. Space of valid parameter configurations for 2 parameters with minima and maxima

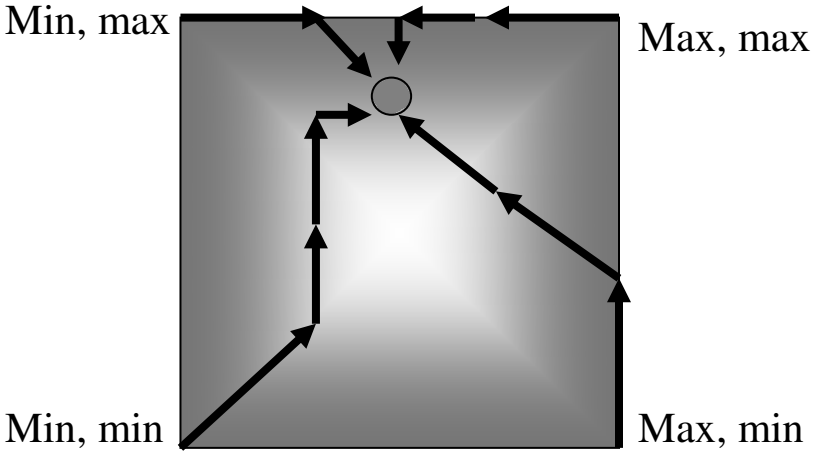

Figure 33. Traversing the parameter space toward the optimum of any given generation (4 generations shown)

Steps associated with the Monte Carlo Method are partly utilized to introduce random parameters within the volume space. This obviates the need for all non-optimum solutions to fully traverse the parameter space. While the initial population of parameters is quite large, fewer generations are necessary to reach an optimum. Furthermore, greater confidence can be achieved in reading a global optimum without stumbling into local extrema.

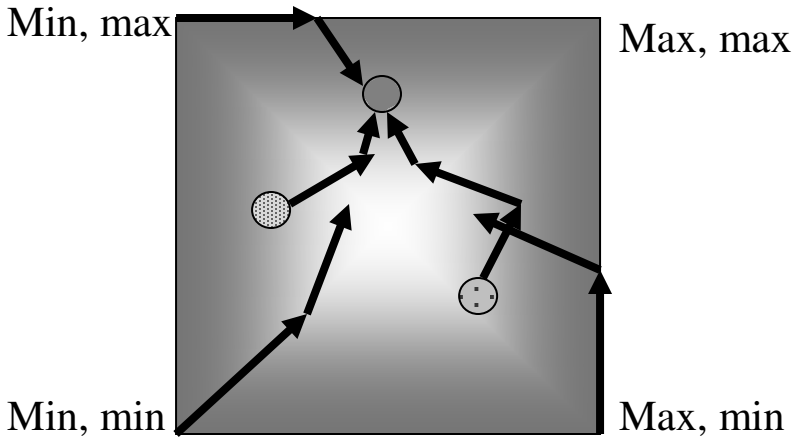

Figure 34. Two random parameter sets are introduced to our hypothetical space (3 generations shown)

While it is desirable to find a balance in utilizing as few analyses as possible while still reaching a global optimum, with greater analyses, comes greater ability to evaluate sensitivity to parameters. Therefore, we accept that a large parameter population benefits us in some aspects while somewhat hindering computation speed.

Table 2. Algorithm Steps

1	Define the parameter upper and lower boundaries
2	Generate a population of all combinations of upper and lower boundaries
3	Introduce a randomized population within the parameter space
4	Evaluate the cost function for each individual and rank by this cost
5	Interpolate the population in the direction of the optimum parameter set from this generation
6	Introduce additional random populations within the parameter space
7	Evaluate each individual in this new generation

At the termination of any given generation, the parameter population is ranked based on cost function. The best parameter set of generation one remains unchanged, while all other individuals within the population are interpolated toward this prime set. Smaller increments will take longer to converge to an ideal solution. Larger increments are more likely to pass over and miss potential optima. It is therefore worthwhile to consider a reasonable increment percentage based on the range of parameters.

$$\begin{aligned} \overline{X}^1(1{:}N, 1{:}M) &= \text{sorted population of generation 1} \\ \overline{X}^2(2{:}N, 1{:}M) &= \left[\overline{X}^1(2{:}N, 1{:}M) - \overline{X}^1(1, 1{:}M)\right] \cdot .75 + \overline{X}^1(1,1{:}M) \end{aligned} \tag{4.3}$$

4.5 Sensitivity

Expressing sensitivity in quantitative terms can be a challenging task. Because the exact nature of the cost function can be difficult to express given the number of parameters, determining a partial derivative with respect to a single parameter may not be readily feasible. There is a high probability of parameter interdependence, and it cannot necessarily be surmised what type or order of equation could be used to describe these relationships. Sensitivity will be expressed in a graph such that a qualitative analysis can take place.

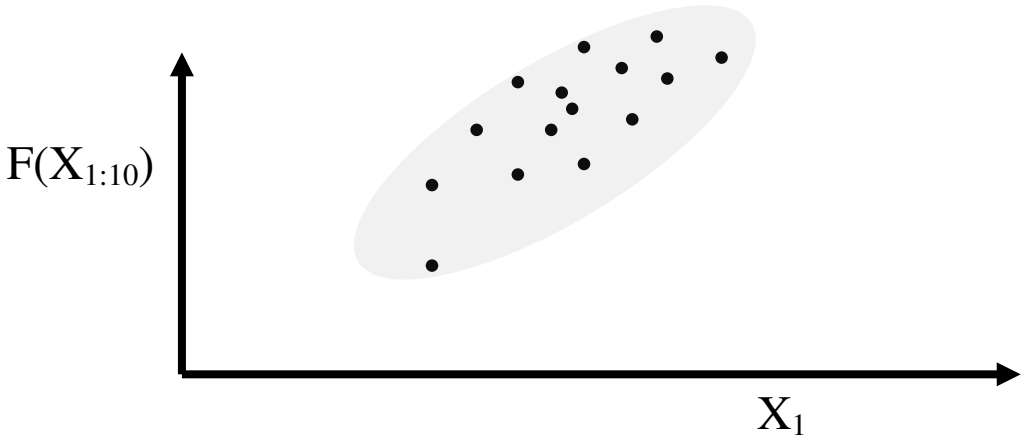

Figure 35. Hypothetical indication of sensitivity by plotting output cost with respect to a particular parameter

In the hypothetical example shown, a clear trend emerges relating output cost to the particular parameter. While some chaos within the data set exists, larger X_1 parameters appear to produce larger costs. From this, combined with all other relationships, relative sensitivities can be expressed to better plan future optimizations without wasting analysis time on conditions highly unlikely to produce low cost output.

From our large finite element data set, for each parameter, we plot the output cost with respect to that particular parameter. The greater the independence of the parameter's effects, the more easily a clear sensitivity trend can be observed. Otherwise, the plot will reveal itself in a shotgun pattern due to its close dependence on other parameters.

5. RESULTS

5.1 Linear Interpolation

The simplest possible finite element initially considered for this analysis is the linear triangular element. These elements can deal with the natural, irregular curvature of the bone and implant. It is of great concern however whether these elements can produce sufficiently accurate stress and deflection data. They are well known to produce overly stiff meshes. Verification is necessary to confirm viability of this element type. If a test analysis produced adequately accurate information, we would be justified in using linear triangular elements.

For a beam 35cm long and 1.0cm by 4.0cm, a 5000N load is axially applied in tension. With a characteristic element size of 3.3mm, over 2800 elements were produced. Comparison between the finite element analysis and theoretical calculations shows excellent accuracy.

Table 3. Finite element analysis using linear triangular elements for axial loading verification

	Theory	FEA	Deviation from Theory
Max Axial Deflection	.4375mm	.445mm	1.7%
Max Normal Stress	12.5MPa	12.5MPa	0%

Even with great confidence in axial loading analysis, similar accuracy in bending is not guaranteed. For the same beam, we now instead apply a pure bending moment of 100Nm. Still using 3.3mm elements, over 2800 elements were again produced. Comparison between

the finite element analysis and theoretical calculations again shows better than 2% deviation from expected values.

Table 4. Finite element analysis using linear triangular elements for bending verification

	Theory	FEA	Deviation from Theory
Max Transverse Deflection	11.48mm	11.3mm	1.57%
Max Normal Stress	37.5MPa	38.12MPa	1.64%

The final verification analysis was carried out to evaluate the effects of an applied shear load. This shear load produces a flexural stress due to bending moment as well as transverse shear stress. As is typical in such loading scenarios, the bending of the beam accounts for much more deflection than the shear distortion. In this situation, there was greater variation for shear stress among elements but for regions of theoretically constant shear stress, an average of several values does produce an excellent approximation.

Table 5. Finite element analysis using linear triangular elements for shear load verification

	Theory	FEA	Deviation from Theory
Max Transverse Deflection	26.8mm	26.7mm	0.37%
Max Normal Stress	131.3MPa	141.9MPa	8.1%
Max Shear Stress	3.75MPa	3.68MPa*	1.87%

These results justify using linear triangular elements to analyze the plane stress of a structure. The simplicity of their expression is of great convenience to our analysis so long as we maintain a sufficiently dense mesh.

5.2 Intact Bone Analysis

With an element edge size of 3.5mm, the finite element model contained almost two thousand nodes within almost four thousand total elements, representing all bone material between the femoral neck and the distal femur. This model is approximately 38cm in length and progresses 17cm beyond the most distal point of the eventual implant location. This additional distance provides ample space for reduction in high stresses due to concentrated loads at the most distal nodes.

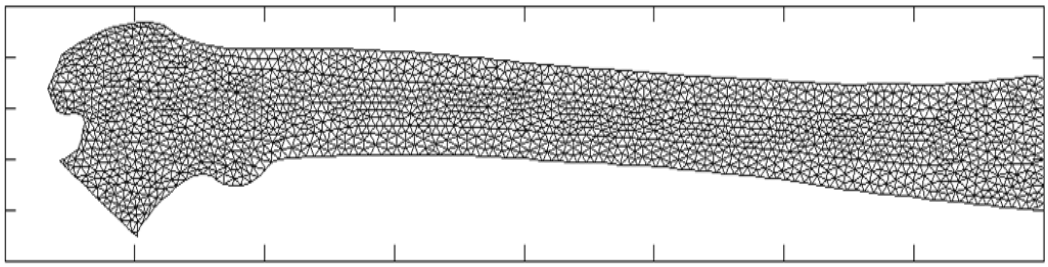

Figure 36. Finite element mesh of the femur

The virtual boundary contains 130 nodes, beginning from the underside of the transverse shoulder plate around the distal shaft and back toward the implant shoulder. At this location on the shoulder, interaction between bone and implant halts since bone at this location is excised prior to surgical implantation.

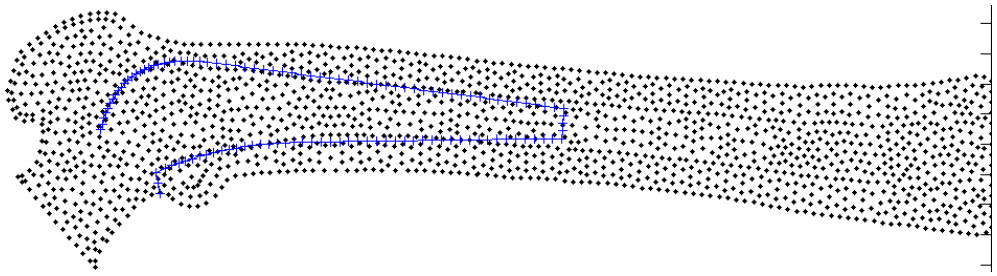

Figure 38. Virtual boundary overlapping the bone nodes

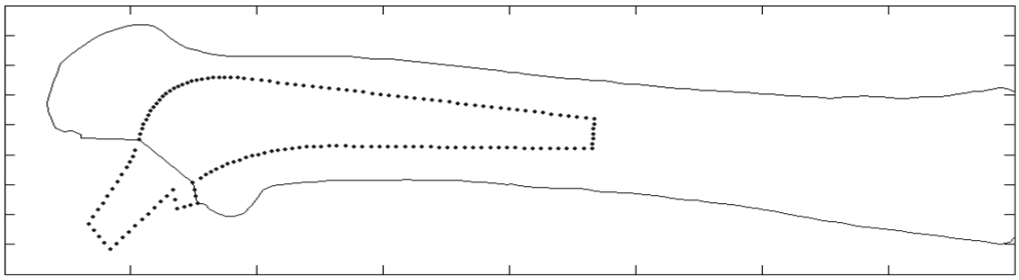

Figure 37. Implantation within bone

From the stresses along the virtual boundary and the normal vectors, normal and shear stresses are defined for the boundary. It is these stresses, as well as the displacements, which are necessary to the subsequent optimization.

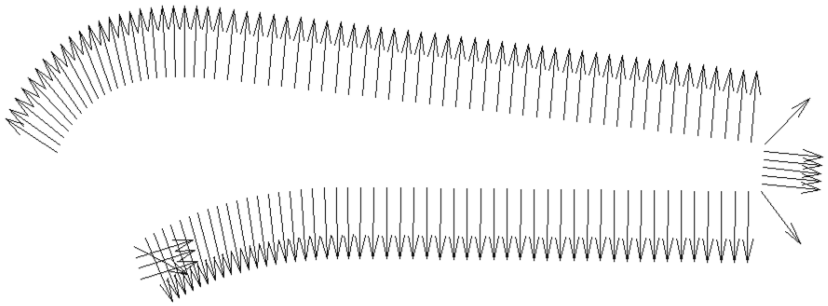

Figure 39. Normal vectors along the virtual boundary

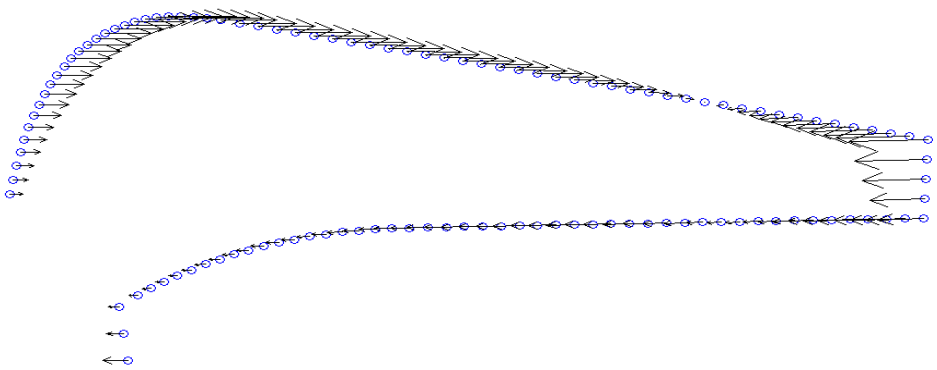

Figure 40. Horizontal deflection applied along the virtual boundary

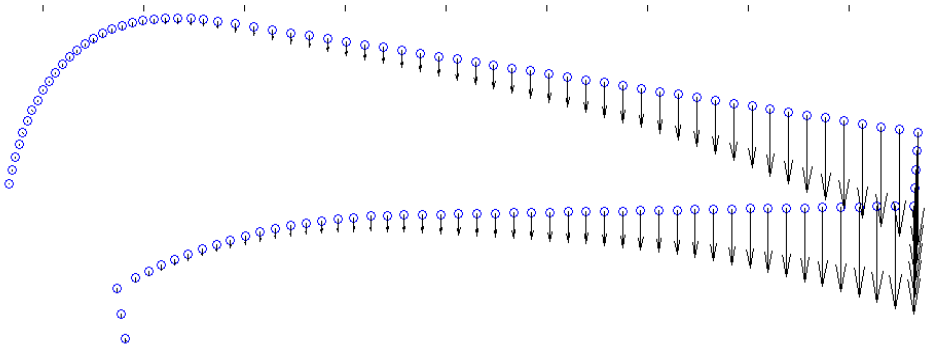

Figure 41. Vertical deflection applied the virtual boundary

5.3 Optimized Geometry

During both load case analyses, eight generations were sufficient for all parameters to approach within 1mm of one another indicating an acceptable implant design. At this point, the standard deviation of the cost among the final population is less than 2% of the average cost value.

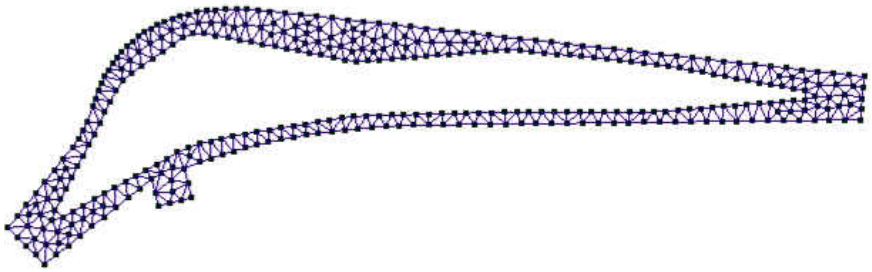

Figure 42. Optimized design given a 3000N load at 10 degrees off axial

Most of the ten parameters were maximized during the optimization, placing them close to the implant outer walls. Several, however, found intermediate values. The removed interior indicated as the optimum design was significant in volume.

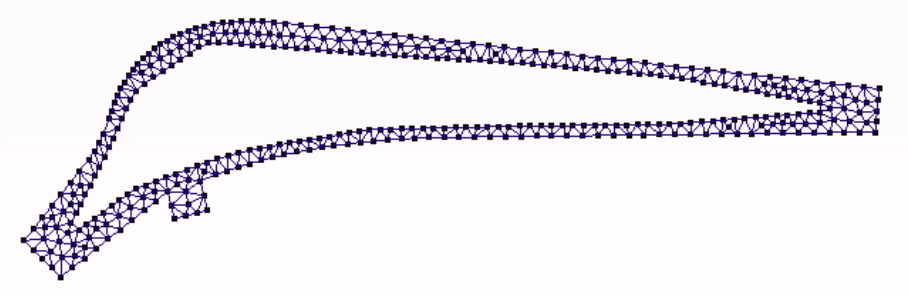

Figure 43. Optimized geometry given a 2300N load at 15 degrees off axial

Table 6. Optimized parameters for case 2

Proximal	Lateral Side	Medial Side
	P1 = 6.032mm	P10=4.776mm
	P2=1.002cm	P9=7.789mm
	P3=8.509mm	P8=1.673cm
	P4=2.372mm	P7=9.065mm
	P5=7.198mm	P6=7.108mm
Distal		

5.4 Sensitivity

Of the ten parameters evaluated, most produced very slight changes in cost. The ten parameters varied throughout the optimization possessed differing degrees of influence over the output cost. Initial observations indicate very low sensitivity to the most proximal and lateral parameters. Distal and medial parameters tended to produce more steep changes in cost.

The greatest sensitivity lies in parameters five and six, the most distal variable parameters in the implant stem. The cost function drops more quickly as these parameters increase to maximum. Parameter nine creates a lesser sensitivity, and the remaining parameters produce very slight changes in cost. This does not mean that the other parameters are not relevant to this analysis – only that the cost changes slightly with these parameters and/or that they are highly coupled with the other parameters.

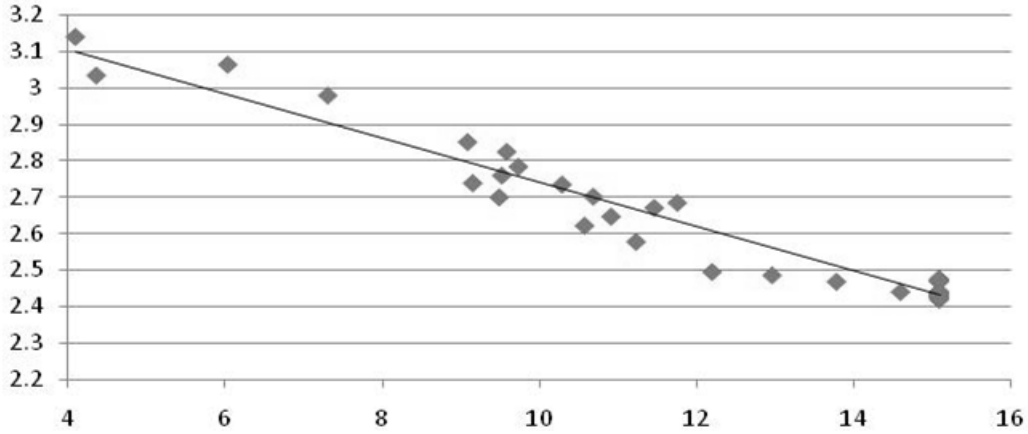

Figure 44. Sensitivity interpreted from graph of cost vs. the sum of parameters 5 & 6

Three models were generated for analysis and verification: an all bone model, a bone model with solid titanium implant, and the optimized implant model. The all bone model is analyzed initially for use in optimization. One of the hollow implant models is based on the recently obtained optimized design. For all of these finite element models, evaluation is based on the stresses within the bone along the implant boundary. This comprises normal and shear stress along the entire surface.

6. CONCLUSIONS

A great number of researchers have attempted to optimize the external geometry or material properties of femoral hip implant stems. There is a great deal of varied success given their diverse assumptions regarding the implant type and bone behavior. While such approaches are undoubtedly useful to the future of hip implant designs, success in utilizing some particular approach certainly does not obviate the ability to incorporate additional approaches to this field. The current work has considered a more unique optimization to evaluate ideal internal geometry of an implant.

Analysis was accomplished by first analyzing two dimensional bone performance under multiple load cases. Behavior (displacement and stress information) was extracted at the virtual boundary – the location of the eventual implant. This behavior was then utilized to examine the implant without coupling it to the bone in a single, large finite element model. The implant was constrained at the neck just as the bone model was constrained. The virtual boundary was forced to displace just as bone had at those same coordinates. Along the surface of the virtual boundary, normal and shear stresses were obtained as they indicate the quality of the design – not by how large or small, but by how they deviated from expected behavior.

The final optimized designs possess thin walls, as expected. The designs noticeably increase flexibility within the implant, allowing greater displacement and, therefore, reduced stresses when displaced. The more an implant is permitted to displace, the more balanced will be the stresses throughout the composite system. It is these effects which lead to reduced

stress shielding within remnant femoral bone – meaning an increase in stresses and a return to normalcy.

It must be noted that no geometry can satisfy all loading patterns. The differences in titanium and bone are still too great and the loading scenarios too diverse to allow for universal long-term harmony. However, the more extreme loading scenarios tend to also be the rarest. As bone remodeling is a slow process, adaptation best reacts to typical usage as averaged over repeated cycles in a given day. The more a person follows typical repetitive loading behavior, the more optimum their remnant bone response will be over time if using the implant configurations presented here. Even an additional year of life would greatly impact the world of THA, justifying the steep uphill climb toward a true optimum implant.

Table 7. Research contributions

1	Successful uncoupling of THA system in order to analyze and optimize femoral implant unaccompanied by bone
2	Validation that flexibility in the shoulder of the implant is highly significant to implant performance
3	Achieved varied, but similar, implant designs for multiple walking loads
4	Rejected isotropy in favor of transversely isotropic cancellous and cortical bone behavior
5	Rejected homogeneous cancellous bone behavior in favor of three regions over the length of the femur

Future work demands more complex analysis of potential internal geometries. Three-dimensional finite element models can take this research further and produce implants with true implantation potential. Using the same considerations as in the present work, additional load conditions could be applied to the bone model to produce a greater range of possible implant configurations (other choices in kinesiology and biomechanical research include stair climbing and standing from sitting). While using each loading condition would produce unique implant geometry, the results will aid in understanding of important geometric considerations as related to the lifestyle of the recipient. All results would be valid for specific physical actions, and it would be the responsibility of the researcher to decide how to weigh those results accordingly.

7. REFERENCES

Anatomy and Biomechanics of the Hip Relevant to Arthroplasty. Johns Hopkins University, Good Samaritan Hospital. <http://aboutjoints.com/physicianinfo/topics/anatomyhip/biomechanicship.htm>.

Anderson, Frank & Pandy, Marcus. "Dynamic Optmization of Human Walking." Journal of Biomechanical Engineering (2001): 381-390.

Bagge, Mette. "A model of bone adaptation as an optimization process." Journal of Biomechanics (2000): 1349-1357.

Beer, Ferdinand P. et al. Mechanics of Materials. 5th. Boston: McGraw Hill , 2006.

Boresi, Arthur P. and Ken P. Chong. Elasticity in Engineering Mechanics. 2nd. New York: John Wiley & Sons, Inc., 2000.

Bouvier, Marianne. "The Biology and Composition of Bone." Bone Mechanics. Ed. Stephen C. Cowin. New York: CRC Press, 1989. 1-14.

Bundy, Kirk J. "Bone Prosthesis and Implants." Bone Mechanics. Ed. Stephen C. Cowin. New York: CRC Press, 1989. 159-196.

Bundy, Kirk J. "Composite Material Models for Bone." Bone Mechanics. Ed. Stephen C. Cowin. New York: CRC Press, 1989. 197-210.

Chang, Paul B. et al. "Design and Analysis of Robust Total Joint Replacements: Finite Element Model Experiments with Environmental Variables." Journal of Biomechanical Engineering 123 (2001): 239-246.

Charnley, J. Low Friction Arthroplasty of the Hip: Theory and Practice. New York: Springer-Verlag Berlin Heidelberg, 1979.

Cowin, Stephen C. "Mechanics of Materials." Bone Mechanics. Ed. Stephen C. Cowin. New York: CRC Press, 1989. 15-42.

Cowin, Stephen C. "The False Premise in Wolff's Law." Bone Mechanics Handbook. Ed. Stephen C. Cowin. 2nd . CRC Press, 2001.

Cowin, Stephen C. "The Mechanical Properties of Cancellous Bone." Bone Mechanics. Ed. Stephen C. Cowin. New York: CRC Press, 1989. 129-158.

Cowin, Stephen C. "The Mechanical Properties of Cortical Bone Tissue." Bone Mechanics. Ed. Stephen C. Cowin. New York: CRC Press, 1989. 97-128.

Cunningham, Robert A. Hip implant prosthesis. United States: Patent 5755810. 26 May 1998.

Cunningham, Robert. "Minimizing Stress Shielding in Hip Implant by Mechanical Design." Advances in Bioengineering 39 (1998): 295-303.

Evans, S.L. & Gregson, P.J. "Numerical optimization of the design of a coated, cementless hip prosthesis." Journal of Materials Science: Materials in Medicine 5 (1994): 507-510.

Fung, Y.C. Biomechanics: Mechanical Properties of Living Tissues. 2nd. New York: Springer, 1993.

Goldstein, S.A. "The Mechanical Properties of Trabecular Bone: Dependence on Anatomic Location and Function." Journal of Biomechanics 20.11/12 (1987): 1055-1061.

Gray, Henry. Gray's Anatomy. 15th. New York: Barnes & Noble Books, 1995.

Hart, Richard T. "The Finite Element Method." Bone Mechanics. Ed. Stephen C. Cowin. New York: CRC Press, 1989. 53-74.

Heller, M. O. et al. "Musculo-skeletal loading conditions at the hip during walking and stair climbing." Journal of Biomechanics 34 (2001): 883-893.

Higa, Masaru et al. "Shape Optimization of Femoral Components of an Artificial Hip Prosthesis Using the Three-Dimensional P-Version Finite Element Method." 2001 ASME International Mechanical Engineering Congress and Exposition. New York, 2001. 25-26.

Hori, R.Y. et al. "An Analysis of 130 Removed Total Hips and Knees." Implant Retrieval, Materials, & Biologic Analysis, National Bureau of Standards Conference. 1980. 509-558.

Huiskes, R. "Adaptive Bone-Remodeling Theory Applied to Prosthetic-Design Analysis." Journal of Biomechanics 20.11/12 (1987): 1135-1150.

Hungerford, David. Total Joint Replacement: The Last Frontier. 2006. Inc. Stryker Howmedica Osteonics. 2011 <http://aboutjoints.com/patientinfo/topics/tjrlastfrontier/tjrlastfrontier.htm>.

Jee, Webster S. S. "Integrated Bone Tissue Physiology: Anatomy and Physiology." Bone Mechanics Handbook. Ed. Stephen C. Cowin. CRC Press, 2001.

Joshi, Makarand G. et al. "Analysis of a femoral hip prosthesis designed to reduce stress shielding." Journal of Biomechanics 33 (2000): 1655-1662.

Katoozian, Hamid and Dwight Davy. "Three-Dimensional Shape Optimization of Femoral Component of Hip Prostheses with Nonlinear Frictional Interface." Journal of Mechanics in Medicine and Biology 4.2 (2004): 161-172.

Katz, J. Lawrence & Meunier, Alain. "The Elastic Anisotropy of Bone." Journal of Biomechanics 20.11/12 (1987): 1063-1070.

Kowalczyk, Piotr. "Design Optimization of Cementless Femoral Hip Prostheses Using Finite Element Analysis." Journal of Biomechanical Engineering 123 (2001).

Kuiper, J.H. & Huiskes, R. "Mathematical Optimization of Elastic Properties: Application to Cementless Hip Stem Design." Journal of Biomechanical Engineering 119 (1997): 166-174.

Li, Chaodi et al. "Failure analysis of composite femoral components for hip arthroplasty." Journal of Rehabilitation Research & Development 40.2 (2003): 131-146.

Majeska, Robert J. "Cell Biology of Bone." Bone Mechanics Handbook. Ed. Stephen C Cowin. 2nd. CRC Press, 2001.

Mandell, Jay A. et al. "A conical- collared intramedullary stem can improve stress transfer and limit micromotion." Clinical Biomechanics 19 (2004): 695-703.

Meade, John B. "The Adaptation of Bone to Mechanical Stress: Experimentation and Current Concepts." Bone Mechanics. Ed. Stephen C. Cowin. New York: CRC Press, 1989. 211-252.

Moore, Keith L. & Dalley, Arthur F. Clinically Oriented Anatomy. 4th. Lippincott Williams & Wilkins, 1999.

Natarajan, Raghu N. et al. "A Relationship Between Stress Shielding and Stem Stiffness in the Proximal Femur After Total Hip Replacement." Advances in Bioengineering, Winter Annual Meeting of ASME. 1990. 307-310.

Pawlikowski, M., K. Skalski and M. Haraburda. "Process of hip joint prosthesis design including bone remodeling phenomenon." Computers & Structures 81 (2003): 887-893.

Pearson, Osbjorn M & Lieberman, Daniel E. "The Aging of Wolff's "Law": Ontogeny and Responses to Mechanical Loading in Cortical Bone." Yearbook of Physical Anthropology 47 (2004): 63-99.

Rahman, A.A. and et al. "Stem Stiffness Optimization and Material Properties Evaluation of the Hip Prosthesis." BED-Vol 28, 1994 Advances in Bioengineering 28 (1994): 203-204.

Reddy, J.N. An Introduction to the Finite Element Method. 2nd. Boston: McGraw-Hill, 1993.

Rhoades, Rodney & Pflanzer, Richard. Human Physiology. 3rd. Fort Worth: Saunders College Publishing, 1996.

Roesler, H. "Some Historical Remarks on the Theory of Cancellous Bone Structure (Wolff's Law)." Mechanical Properties of Bone 45 (1981).

Serbousek, Jon et al. Reduced Stiffness Femoral Hip Implant. USA: Patent 5336265. 9 August 1994.

Silva, Leandro de Macedo Soares et al. "Elasticity and Viscoelasticity of Human Tibial Cortical Bone Measured by Nanoindentation." Structure and Mechanical Behavior of Biological Materials. Materials Research Society, 2005.

Simoes, J.A.O et al. "Preliminary investigation of a novel controlled stiffness proximal femoral prosthesis." Proc Instn Mech Engrs. 1998. 165-175.

Smith, Todd S. Controlled Stiffness Femoral Hip Implant. USA: Patent 4808186. 28 February 1989.

Thongpreda, Nisra et al. Implant Fixation System. USA: Patent 5702482. 30 December 1997.

Van Buskirk, W.C. & Ashman, R.B. "The Elastic Moduli of Bone." The Mechanical Properties of Bone (1981): 131-143.

Wuh, Hank et al. "Strain Analysis of the Proximal Femur After Total Hip Replacement." Quantitative Characterization and Performance of Porous Implants for Hard Tissue Applications (1987): 249-263.

Yildiz, Hasan et al. "Composite hip prosthesis design. I. Analysis." Journal of Biomedical Materials Research Volume 39 (1996): 92-101.

Zakeri, Nasser & Katoozian, Hamid. "Optimal Design of a Hip Joint Implant with Hollow Stem Using Finite Element Method." 8th Biennial ASME Conference on Engineering Systems Design and Analysis. Torino, 2006. 505-510.